Journal of
Composites Science

MDPI

Review

Advances in the Integration of Artificial Intelligence and Ultrasonic Techniques for Monitoring Concrete Structures: A Comprehensive Review

Giovanni Angiulli [1,*], Pietro Burrascano [2], Marco Ricci [3] and Mario Versaci [4]

[1] Department of Information Engineering, Infrastructures and Sustainable Energy, Mediterranea University, Via Zehender, I-89122 Reggio Calabria, Italy
[2] Dipartimento di Ingegneria, Università di Perugia, I-05100 Terni, Italy; pietro.burrascano@unipg.it
[3] Department of Computer Engineering, Modeling, Electronics and Systems, Università della Calabria, Viale P. Bucci, Arcavacata di Rende, I-87036 Cosenza, Italy; marco.ricci@unical.it
[4] Department of Civil, Energetic, Environmental and Material Engineering, Mediterranea University, Via Zehender, I-89122 Reggio Calabria, Italy; mario.versaci@unirc.it
* Correspondence: giovanni.angiulli@unirc.it

Abstract: This review examines the integration of advanced ultrasonic techniques and artificial intelligence (AI) for monitoring and analyzing concrete structures, focusing on detecting and classifying internal defects. Concrete structures are subject to damage over time due to environmental factors and dynamic loads, compromising their integrity. Non-destructive techniques, such as ultrasonics, allow for identifying discontinuities and microcracks without altering structural functionality. This review addresses key scientific challenges, such as the complexity of managing the large volumes of data generated by high-resolution inspections and the importance of non-linear models, such as the Hammerstein model, for interpreting ultrasonic signals. Integrating AI with advanced analytical models enhances early defect diagnosis and enables the creation of detailed maps of internal discontinuities. Results reported in the literature show significant improvements in diagnostic sensitivity (up to 30% compared to traditional linear techniques), accuracy in defect localization (improvements of 25%), and reductions in predictive maintenance costs by 20–40%, thanks to advanced systems based on convolutional neural networks and fuzzy logic. These innovative approaches contribute to the sustainability and safety of infrastructure, with significant implications for monitoring and maintaining the built environment. The scientific significance of this review lies in offering a systematic overview of emerging technologies and their application to concrete structures, providing tools to address challenges related to infrastructure degradation and contributing to advancements in composite sciences.

Keywords: ultrasonic techniques; artificial intelligence; structural monitoring; Hammerstein model; non-destructive testing (NDT); concrete microcracks; signal processing; predictive maintenance

Citation: Angiulli, G.; Burrascano, P.; Ricci, M.; Versaci, M. Advances in the Integration of Artificial Intelligence and Ultrasonic Techniques for Monitoring Concrete Structures: A Comprehensive Review. *J. Compos. Sci.* **2024**, *8*, 531. https://doi.org/10.3390/jcs8120531

Academic Editor: Peng Zhang

Received: 16 November 2024
Revised: 9 December 2024
Accepted: 12 December 2024
Published: 15 December 2024

1. Introduction

Concrete structures are vulnerable to damage due to environmental factors and dynamic loads [1–3]. Non-destructive techniques (NDTs) provide highly effective and accurate tools for detecting the presence of any discontinuities that have formed as a result of the stresses to which the structure is subjected. These techniques are based on an analysis of the propagation in the structure to be investigated. The use of self-healing concrete offers an innovative solution, activating mechanisms that limit damage and reduce external interventions [4–7]. Before analyzing propagation in self-healing concrete, it is essential to acquire a clear understanding of innovative models and algorithms for the localization, classification, and prediction of defects, capable of highlighting structural non-linearities and effectively managing large volumes of data. However, the precise evaluation of structures requires

advanced monitoring techniques to detect defects early and predict their evolution [8–10]. Non-destructive techniques (NDTs) allow for monitoring the integrity of structures without compromising their functionality [11–21], unlike destructive tests [22–26].

Among the most common NDTs, thermography identifies superficial anomalies but does not detect deep defects [27–32]. X-ray analyses offer detailed images but require expensive equipment with exposure risks [33–36], while vibrational measurements are limited in detecting minor defects [37–39]. Ultrasonic (US) techniques penetrate deep into the concrete, detecting microcracks and internal discontinuities with high precision [40–45].

The discontinuities alter the path of the US, highlighting non-linear behaviors detected through complex models such as that of Hammerstein [46], which allows the early detection of cracks with greater sensitivity than linear techniques. However, managing US data is complex as the phenomenon is governed by numerous [47–50] variables. Artificial intelligence (AI) supports processing this data, improving structural safety and reducing maintenance expenses, and enables early diagnosis of defects by detecting weak signals that escape conventional analysis.

The research project "Integration of Artificial Intelligence and Ultrasonic Techniques for Monitoring Control and Self-Repair of Civil Concrete Structures (CAIUS)", which lasts 24 months and is funded by the Italian Ministry of University and Research (MUR) under the PRIN 2022 program (Prot. 2022AZPLL8), integrates AI and US to develop advanced models based on fuzzy logic. These models obtain high-resolution maps of discontinuities in concrete and monitor self-healing processes in civil concrete structures. The synergy between the Hammerstein model and AI allows us to accurately describe US propagation, improving the detection and evaluation of defects [46,50].

Key features of CAIUS include developing defect maps based on non-linear US techniques, creating neuro-fuzzy predictive models for structural risk analysis, and optimizing AI algorithms for processing large data sets. The project also involves laboratory testing on specimens using self-repair techniques with innovative cementitious materials enriched with crystallizing additives and field testing on existing structures.

CAIUS stands out for its design of real-time monitoring systems with low computational load and its wireless device remote control capability. Its interdisciplinary approach involves advanced expertise in civil engineering, AI, and non-destructive testing techniques, ensuring a significant scientific, technological, and societal impact. The project aligns closely with the National Recovery and Resilience Plan (PNRR) objectives, contributing to the safety, sustainability, and redevelopment of the national infrastructure.

The synergy between Hammerstein models and AI creates a continuous monitoring system essential for predictive maintenance, reducing costs, and evaluating the effectiveness of self-repair processes. The CAIUS project, thus conceived, associates each US signal with a specific defect type, creating an abacus of defects that will constitute a valuable reference for technicians and legislators for any updates to the current legislation. CAIUS thus responds to the global need for infrastructure safety and the growing attention towards self-healing concrete, contributing to the long-term sustainability of structures.

The main objectives of this review can be summarized as follows. To conduct an in-depth scientific review on high-resolution US technologies and the use of AI, integrating non-linear Hammerstein models to manage data and create an effective structural monitoring system and integrating Hammerstein models with AI to analyze high-resolution US wave propagation in concrete address intrinsic non-linearities, enhancing sensitivity, detection, classification, and defect prediction. This approach creates an efficient and durable monitoring system that reduces maintenance expenses by leveraging hybrid systems based on fuzzy logic, enabling intuitive data management through adaptable and easily updatable fuzzy rule banks by experts.

Our aim is to offer a complete overview of concrete monitoring that can also be used for self-repairing concretes, with tools for real-time analysis.

Given that high-resolution ultrasonic (US) techniques generate large volumes of data, often affected by noise, the most suitable filtering methodologies will be analyzed to

enhance the interpretive accuracy of US signals. This analysis is automated through convolutional neural networks, which detect potential microcracks that, using AI-based approaches, can be monitored to estimate the risk of further damage and/or the need for interventions. The review emphasizes how integrating US and AI techniques facilitates managing large data volumes, enhancing noise filtering, and optimizing US data interpretation. This approach advances structural diagnostics, offering a detailed understanding of concrete conditions and improving predictive maintenance efficiency. The CAIUS project significantly contributes to preventive maintenance solutions and cost reduction, and establishes itself as a reference for future AI-driven infrastructure monitoring research. Figure 1 displays a flow chart of this work, also highlighting the link between what is proposed and the corresponding section.

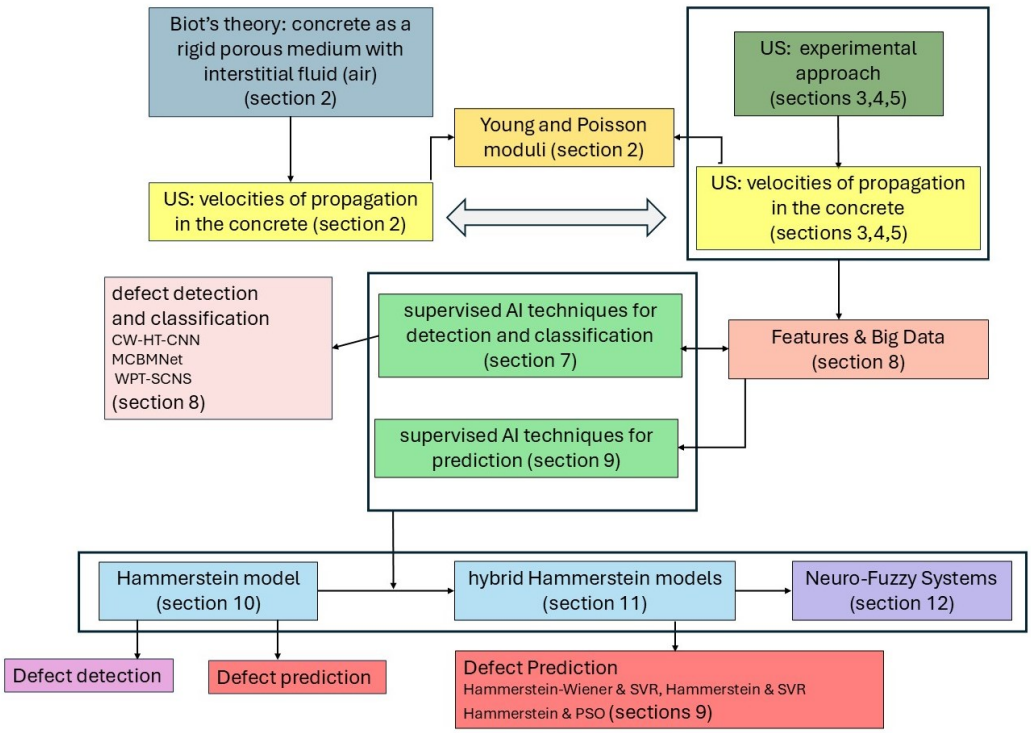

Figure 1. Visual abstract summarizing the logical organization of this review: Based on Biot's theory and, in parallel with the experimental investigation, the comparable values of the US wave speed allow the evaluation of the Young and Poisson modules. The large amount of data available require AI techniques for detecting, classifying, and predicting defects. Furthermore, using Hammerstein models combined with appropriate AI techniques allows for obtaining performances that are a prelude to an effective and efficient synergy with neuro-fuzzy systems.

The remaining part of the review is structured as follows. Once the main ones have been outlined, the physical–mathematical foundations of US in NDT are finished (Section 2) as they pertain to US in concrete (intended as porous media according to Biot's theory), also regarding the mechanical characteristics of concrete as a function of US propagation speeds. Section 3 specifies the methods for carrying out laboratory tests on "ad hoc" constructed specimens, also discussing the attenuation problem (Section 4 below). Once the issue of non-linearity is introduced (Section 5), modern high-resolution US technologies that exhibit the well-known problem of "big data" are discussed in Sections 6 and 7, highlights how some supervised AI techniques equipped with learning procedures locate and classify defects in concrete via US, just as some types of transforms assist back-propagation neural networks in structuring neural architectures, which can be optimized using genetic algorithms, to achieve the objectives set (Section 8). Furthermore, Section 9 proposes some supervised AI techniques for the prediction of defects in concrete using the US and then

introduces the Hammerstein model, which is helpful in the localization, classification, and evolution of defects (Section 10). The next section (Section 11) proposes some of the most advanced synergies between the Hammerstein model and AI techniques for improving performance. Then, the paper converges on a section proposed in the CAIUS Project, which integrates the Hammerstein models with approaches to fuzzy ascription in network mode to take advantage of innovative learning algorithms (Section 12). Finally, some conclusions and future perspectives are offered as helpful food for thought for the continuation of scientific activity.

2. Fundamentals of Mathematical Physics for the Application of US in NDT

Since concrete is a porous medium with air present in the pores, Biot's theory of poroelasticity can describe the propagation of US waves, but the physical properties of air influence the propagation differently compared to a denser fluid (such as water) [51–54].

The oscillations are elastically transmitted from one area of the material to the next as a wave characterized by directions of propagation and vibration. If the wave is longitudinal, the direction of vibration is parallel to that of propagation: the elementary particles, arranged on an ideal plane, cyclically increase and decrease their distance regarding the next plane, creating areas of pressure and depression. They propagate in solids, liquids, and gases, are characterized by acoustic pressure (force per unit of surface area exerted perpendicularly to the wave-front), and constitute the type most commonly used in US inspection. In transverse waves, the direction of vibration is perpendicular to that of propagation, and they are used for US inspection of welded joints propagating exclusively in solid media since gases and liquids do not transmit shear stresses (but only compressive stresses). Surface waves propagate only in the outermost layers of materials (thickness of the order of $1 \div 2$ wavelengths).

Biot's theory models the propagation of US waves through concrete via solid–fluid interactions in porous materials. Unlike alternative theories that could consider the material only as solid or fluid (Johnson-Allard [55], Kuster-Toksöz [56]), Biot distinguishes between the movements of the solid matrix and the fluid in the pores, allowing for accurately describing the presence of multiple wave modes and the viscous and inertial effects that influence wave speed and attenuation. Biot's theory, valid over a broad frequency spectrum and confirmed by empirical research, proves flexible and accurate in describing ultrasonic propagation in concrete, allowing it to adapt to different boundary conditions and complex geometries for engineering applications.

The equation of motion for the solid matrix, derived from Newton's law for the dynamics of a porous medium, is as follows [51–54]:

$$\rho_{11}\frac{\partial^2 \mathbf{u}}{\partial t^2} + \rho_{12}\frac{\partial^2 \mathbf{w}}{\partial t^2} = \nabla \cdot \boldsymbol{\sigma} + \alpha \nabla P \tag{1}$$

where $\mathbf{u}$ [m] is the displacement of the solid matrix; $\mathbf{w}$ [m] is the relative displacement of the air in the pores; $\rho_{11} = \rho_s + \phi\rho_f$ [kg/m^3] is the effective density of the solid matrix, where ρ_s [kg/m^3] is the density of the solid matrix and ϕ (dimensionless) is the porosity of the material, and ρ_f [kg/m^3] is the density of the air (equal to approximately 1.2 kg/m^3). Furthermore, $\rho_{12} = -\phi\rho_f$ [kg/m^3] is the dynamic coupling term between the solid matrix and the air in the pores, while σ [Pa] is the stress tensor in the solid matrix. Finally, α (dimensionless) is the coupling coefficient between the pore air pressure and the matrix deformation. Obviously, P [Pa] indicates the air pressure in the pores.

The air in the pores obeys the following equation of motion [51–54,57]:

$$\rho_{12}\frac{\partial^2 \mathbf{u}}{\partial t^2} + \rho_{22}\frac{\partial^2 \mathbf{w}}{\partial t^2} = \nabla P - \alpha \nabla \cdot \boldsymbol{\sigma} - \eta \mathbf{w} \tag{2}$$

where $\rho_{22} = \phi\rho_f$ [kg/m^3] is the density of the air in the pores; η [Pa·s] is the dynamic viscosity of air (1.81×10^{-5} Pa·s at room temperature).

P is related to the volumetric compression of the solid matrix and the fluid through the following [51–54]:

$$P = -M(\nabla \cdot \mathbf{u} + \nabla \cdot \mathbf{w}) \tag{3}$$

where M [Pa] is the compressibility modulus of the air (capacity of the air to be compressed inside the pores), evaluated as $M = S^{-1}\gamma P_0$, where γ (dimensionless) is the ratio of the specific heats of the air (about 1.4), P_0 [Pa] is the atmospheric pressure (equal to about 101,325 Pa) and S is the saturation of air in the pores.

Since $\rho_f \ll \rho_s$, Equation (2), for our specific case, is negligible. Then, the acceleration term, $\rho_{22}\frac{\partial^2 \mathbf{w}}{\partial t^2}$, is minimal compared to the terms associated with the solid matrix. Furthermore, the coupling term, $\alpha\nabla \cdot \boldsymbol{\sigma}$, representing the interaction between the air in the pores and the deformation of the solid matrix, given the low density and viscosity of the air, is weak compared to other elastic effects. Finally, $\mathbf{w}$ is small compared to $\mathbf{u}$, so we approximate $\mathbf{w}$ as follows [51–54]:

$$\mathbf{w} \approx -\frac{\rho_{12}}{\rho_{22}}\mathbf{u}. \tag{4}$$

Then, substituting (4) into (1), we obtain the following:

$$\rho_{11}\frac{\partial^2 \mathbf{u}}{\partial t^2} - \frac{\rho_{12}^2}{\rho_{22}}\frac{\partial^2 \mathbf{u}}{\partial t^2} = \nabla \cdot \boldsymbol{\sigma} - \alpha M \nabla\left(\nabla \cdot \mathbf{u} - \frac{\rho_{12}}{\rho_{22}}\nabla \cdot \mathbf{u}\right) \tag{5}$$

Hence, as in [51–54], it can be seen that

$$\rho_{\text{eff}} = \rho_{11} - \frac{\rho_{12}^2}{\rho_{22}} \tag{6}$$

For the effective density, we obtain the following [51–54]:

$$\rho_{\text{eff}}\frac{\partial^2 \mathbf{u}}{\partial t^2} = \nabla \cdot \boldsymbol{\sigma} - \alpha M \nabla\left(1 - \frac{\rho_{12}}{\rho_{22}}\right)\nabla \cdot \mathbf{u}. \tag{7}$$

But from continuum mechanics, the constitutive relation for the efforts takes the following form [51–54]:

$$\boldsymbol{\sigma} = 2G\mathbf{e} + \lambda(\nabla \cdot \mathbf{u})\mathbf{I}, \qquad \mathbf{e} = \frac{1}{2}\left(\nabla\mathbf{u} + \nabla\mathbf{u}^T\right) \tag{8}$$

where $\mathbf{e}$ represents the strain tensor, G [Pa] is the shear modulus of the solid matrix (which for concrete is of the order of 10^9 Pa); λ [Pa] is the first Lamé parameter (a measure of the volumetric resistance of the material and describes how the material reacts to a change in volume under compression or expansion). Then, substituting the first of the (8) into (7), we obtain that

$$\rho_{\text{eff}}\frac{\partial^2 \mathbf{u}}{\partial t^2} = \nabla \cdot (2G\mathbf{e} + \lambda(\nabla \cdot \mathbf{u})\mathbf{I}) - \alpha M \nabla\left(1 - \frac{\rho_{12}}{\rho_{22}}\right)\nabla \cdot \mathbf{u}. \tag{9}$$

We observe that α, coupling the air pressure and the deformation of the solid matrix, for elastic waves where the interaction between the solid matrix and the air is negligible, decreases considerably because ρ_f is very low compared to the solid matrix, which reduces the dynamic contribution of the air.

Furthermore, when $\rho_{12} \ll \rho_{22}$, $1 - \frac{\rho_{12}}{\rho_{22}} \to 1$, it is implied that $\alpha M\nabla(1 - \frac{\rho_{12}}{\rho_{22}})\nabla \cdot \mathbf{u} \approx M\nabla(\nabla \cdot \mathbf{u})$. However, since the solid matrix is dominant, the term with α disappears from Equation (9), with the positive sign remaining because the compression, associated with the pressure of the fluid, is positive, assuming the following final form [51–54]:

$$\nabla \cdot (2G\mathbf{e} + \lambda(\nabla \cdot \mathbf{u})\mathbf{I}) + M\nabla(\nabla \cdot \mathbf{u}) = \rho_{\text{eff}}\frac{\partial^2 \mathbf{u}}{\partial t^2}. \tag{10}$$

In the case of longitudinal waves, $\mathbf{u}$ is a scalar function that varies only along a specific direction, $\mathbf{u} = u(x,t)\mathbf{e}_x$, where $\mathbf{e}_x$ is the unit vector of the direction of wave propagation so that the shear components of $\mathbf{e}$ do not contribute to the motion. In the first of (8), $2G\mathbf{e}$, which represents the shear stresses, since $\mathbf{e}$ has only diagonal components, contributes only to the volumetric compression. $\lambda(\nabla \cdot \mathbf{u})\mathbf{I}$, describing the volumetric part of the effort, depends on $\nabla \cdot \mathbf{u}$. Then, combining the terms, $\boldsymbol{\sigma} = (\lambda + 2G)(\nabla \cdot \mathbf{u})\mathbf{I}$ [51–54]. Furthermore, since $\mathbf{e}$ contributes only to volumetric compression, $M\nabla(\nabla \cdot \mathbf{u})$ represents the contribution of the compressibility modulus of the air in the pores; then, it can be neglected if the influence of air in the pores is weak compared to the elastic behavior of the solid matrix. Finally, (10) becomes the following [51–54]:

$$\nabla \cdot ((\lambda + 2G)(\nabla \cdot \mathbf{u})\mathbf{I}) = \rho_{\text{eff}} \frac{\partial^2 \mathbf{u}}{\partial t^2}, \tag{11}$$

which, given the scalarity of $\mathbf{u}$, $\nabla \cdot \mathbf{u} = \nabla \cdot u$, takes the following form: [51–54]:

$$(\lambda + 2G)\nabla(\nabla \cdot u) = \rho_{\text{eff}} \frac{\partial^2 u}{\partial t^2}. \tag{12}$$

Using the hyperbolic Equation (12), it is necessary to consider appropriate initial and boundary conditions for the specimen dependent on the mechanical properties of the concrete (including λ, G, and ρ_{eff}) and under specific geometric and physical conditions [51–54]. A usual choice is to assume that the material is initially in a state of rest, $u(\mathbf{x}, 0) = 0$, applying a US source which at $t = 0$ has a non-zero initial velocity, $\frac{\partial u}{\partial t}(\mathbf{x}, 0) = f(\mathbf{x})$, where $f(\mathbf{x})$ represents the initial distribution of the speed imparted by the US source [51].

If the specimen surface is not confined or constrained, it makes sense to impose [51] $\boldsymbol{\sigma} \cdot \mathbf{n} = 0$ on $\partial\Omega$ where $\mathbf{n}$ is the unit vector normal to the $\partial\Omega$ of the specimen. In terms of displacement, the above condition can be translated as $\frac{\partial u}{\partial n} = 0$, i.e., that the displacement gradient normal to the surface is zero. If one of the faces of the specimen is constrained or in contact with a rigid surface, $u = 0$ can be imposed on $\partial\Omega$ [51].

To avoid unwanted reflections at the ends, an absorption condition is imposed at the far ends, representing the wave's dissipation. This condition allows the wave to exit the domain without reflection, $\frac{\partial u}{\partial t} + c\frac{\partial u}{\partial n} = 0$, imitating the behavior of a material which absorbs the energy of the waves [52].

The initial and boundary conditions defined for the concrete specimen guarantee a unique and realistic solution. A stable system is obtained by establishing a precise initial state and specifying consistent physical constraints for the unconstrained and rigid surfaces. The absorption condition at the ends avoids unwanted reflections, ensuring natural wave propagation and preventing interference that could compromise the uniqueness of the solution. The speed of sound within concrete provides information about its internal structure and defects. It also influences the elastic properties of the material (Poisson's ratio and Young's modulus), which define the mechanical response of the material stressed. Suppose we assume that the speed of the compression waves (longitudinal waves or P waves) in the supposedly elastic and isotropic material is given by the following [58]:

$$c = \sqrt{(\rho_{\text{eff}})^{-1}(\lambda + 2G)} \tag{13}$$

where c [m/s] is the speed of wave propagation. Thus, by substituting (13) into (12), we obtain the classical equation of wave propagation in a continuous and isotropic elastic medium [58]:

$$\frac{\partial^2 u}{\partial t^2} = c^2 \nabla^2 u. \tag{14}$$

P and S wave velocities provide detailed information about the internal structure and integrity of concrete. The velocity of the P waves, v_p [m/s], depends on the elastic properties of the material, in particular on G and on ρ_{eff} [52,58]:

$$v_P = \sqrt{(\rho_{\text{eff}})^{-1}(K + 1.33)} \tag{15}$$

where K [Pa] is the compressibility modulus, which evaluates the resistance of the concrete to volumetric compression. P waves, traveling faster than S waves, are the first to be detected by sensors and allow the identification of internal defects (voids, porosity, inclusions), offering indications on the quality of the material in terms of integrity and resistance. S waves propagate in concrete by causing the particles to oscillate perpendicular to the direction of propagation. The speed of the S waves, v_S, is closely related to the resistance of the material to transverse deformation expressed by the following [58]:

$$v_S = \sqrt{\rho_{\text{eff}}^{-1} G} \tag{16}$$

S waves travel more slowly than P waves, providing useful information on internal defects, especially micro-cracks and oriented discontinuities such as cracks and dislocations that escape P wave analysis.

The combined analysis of v_S and v_P allows calculating the dimensionless Poisson modulus ν, which describes the ratio between the transverse and longitudinal deformation when the concrete is subjected to compression or traction. It can be calculated by the following [58]:

$$\nu = 2(v_P^2 - v_S^2)(v_P^2 - 2v_S^2), \tag{17}$$

from which we obtain Young's modulus [Pa], $E = 2G(1 + \nu)$, which represents a measure of the stiffness of the concrete and describes its ability to resist elastic deformation when subjected to a stress along an axis. Since v_P and v_S are influenced by different factors (composition of the material, porosity, degree of saturation). The presence of aggregates, water, or air in the pores significantly influences the speed of the waves. The viscosity of the fluid in the pores and the ultrasonic frequency attenuate the US waves. The phenomenon can be described by the attenuation coefficient, α_{att} [1/m], which can be evaluated according to [51,52,58], as $\alpha_{\text{att}} = \frac{\omega}{Q}$, where ω [rad/s] is the angular frequency of the US waves; Q (dimensionless) is the material quality factor (ratio between stored and dissipated energy). Dually, it is possible to obtain v_P and v_S starting from E and ν. In fact, following [58], considering that

$$G = (2(1 + \nu))^{-1} E, \qquad K = \frac{E}{3(1 - 2\nu)}, \tag{18}$$

(15) becomes the following [58]:

$$v_P = \sqrt{\frac{\frac{E}{3(1-2\nu)} + \frac{4}{3}\frac{E}{2(1+\nu)}}{\rho_{\text{eff}}}} = \sqrt{\frac{E(1-\nu)}{\rho_{\text{eff}}(1+\nu)(1-2\nu)}}. \tag{19}$$

Furthermore, by replacing (18) in (15), it is easy to obtain the following [58]:

$$v_S = \sqrt{\frac{\frac{E}{2(1+\nu)}}{\rho_{\text{eff}}}} = \sqrt{\frac{E}{2\rho_{\text{eff}}(1+\nu)}}. \tag{20}$$

The US signal exploits the ability of some crystals to vibrate under the action of an electric field **E** producing elastic waves of US frequency, as long as **E** oscillates at the resonance frequency (piezoelectricity) [59]. Since they have a very short wavelengths, US signals can be reflected from minimal surfaces (defects). US probes, transducers that convert electrical

impulses into mechanical vibrations and vice versa, are made of a piezoelectric material consisting of a sheet of polarized material. Applying an electric voltage generates a field **E** so that the polarized molecules align themselves parallel to **E**, causing the material to expand, transforming the electrical energy into deformation energy.

The main investigation techniques are "through transmission" and "pulse-echo" techniques, which involve three different methods of US inspection: direct, semi-direct, or indirect.

The direct mode uses two probes arranged on opposite surfaces of the specimen, aligned with each other (see Figure 2a). The emitting probe, via a pulser-receiver, generates US waves by applying an impulsive voltage to the sheet of polarized material, which, when deformed, begins to vibrate and generate US waves transmitted to the specimen by contact. The receiving probe, initially at rest, resting on the opposite surface of the material under examination, receives, again by contact, the train of waves generated, thus starting to vibrate (if the vibration frequencies of the probes coincide). The sheet of polarized material vibrates and produces voltage pulses that are transmitted to the pulser receivers. Pulse receivers, probes, and a PC station (or an oscilloscope) constitute the basic equipment used for US inspection. On the other hand, the receiver section receives the voltage signals sent by the transducer (receiving probe) and amplifies them, making them available at the output as radio frequency. Through a coupling medium with reduced absorption, the US waves impact the concrete and, propagating at the generator's frequency, hit the defect, absorbing energy and emitting elastic waves with a frequency typical of its resonance but variously out of phase. The signal that returns to the probe is the superposition of many waves of the same frequency but out of phase and others of different frequencies, also out of phase with each other, containing all the information on the defect's dimensions, geometry, and nature. Figure 2a displays a typical US test on a concrete specimen. The transmitting and receiving probes, positioned along two parallel faces of the specimen, slide in parallel, producing a US signal incident on the specimen. A typical US signal provided by the probes displayed in Figure 2a is shown in Figure 2b, where both the echo due to the defect and the background echo are clearly visible (unwanted signal due to internal reflections of the concrete).

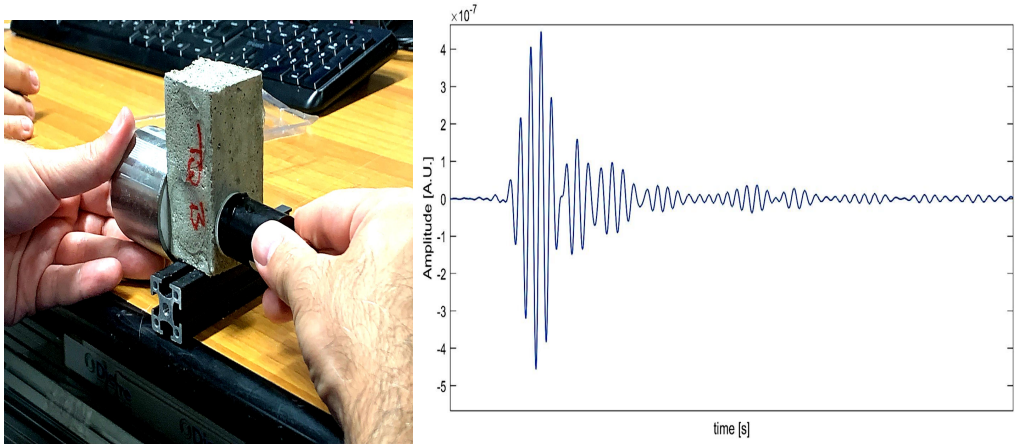

(**a**) (**b**)

Figure 2. (**a**) Typical US test on a concrete specimen. The probe transmitter and receiver flow in parallel to generate a US signal indicative of the concrete's integrity state. (**b**) Representation of the defect echo and the background echo.

Once the process of generating US waves has been described, it is crucial to understand how these waves interact with internal discontinuities within the material. The acoustic impedance of the concrete and its defects determines the amount of wave reflected or transmitted at each discontinuity surface, enabling the identification and characterization of defects.

The acoustic impedance, $Z = \rho_{\text{eff}} v$ [kg/(m^2·s)], with v [m/s] speed of sound (P or S waves) in the material, describes how US waves interact with the boundaries between different materials present in the concrete. When a US wave hits a discontinuity surface, part of the wave is reflected and partly transmitted. The extent of reflection and transmission is determined by the acoustic impedance of the two materials through the reflection coefficient, R, and the transmission coefficient, T [60]:

$$R = \frac{Z_2 - Z_1}{Z_2 + Z_1}, \quad T = \frac{2Z_2}{Z_2 + Z_1} \tag{21}$$

where Z_1 and Z_2 represent the acoustic impedance on the sides of the discontinuity surface. In particular, voids have a much lower Z than solid concrete, reflecting most of the waves. On the other hand, inclusions may have different Z from the surrounding cement paste, causing partial reflections detectable by sensors. Analyzing the reflected and transmitted signals makes it possible to locate defects or discontinuities and evaluate their size and severity.

Remark 1. *Biot's theory is fundamental to physics-informed models. It improves the accuracy of ultrasonic simulations by integrating physical principles into AI models. Thanks to the physical constraints of concrete, this approach enables more precise predictions even with limited data, supporting advanced analyses and more reliable diagnoses, as in the CAIUS project for continuous monitoring and self-healing.*

3. Execution of Tests and Instrumentation Used

To prepare the specimen correctly, mix the ingredients for 2–5 min, paying attention to the water/cement ratio so that it is between 0.4 and 0.6 until a uniform mixture is obtained. The concrete is then poured into lubricated molds and filled into compacted layers to eliminate air bubbles and ensure optimal density. Afterward, the specimens rest for 24 h in the molds, are covered to avoid evaporation, and are kept at a temperature between 20 °C and 25 °C. Subsequently, the specimens are matured for 28 days at a controlled temperature to avoid drying or deterioration. Then, the samples are stored in a controlled environment with a temperature between 20 °C and 25 °C and a relative humidity of 95%. Before testing, surfaces must be cleaned and smoothed. It is essential to document each stage of preparation, including maturation times and environmental conditions, to ensure the traceability and repeatability of the tests.

4. Attenuation of US Wave in Concrete

The absorption, dispersion, and reflection of the ultrasonic wave (US) in concrete progressively reduce its amplitude during propagation. Absorption, due to the viscosity and internal bonds of the material, involves a loss of energy, which causes an exponential decrease in the wave's amplitude with the distance traveled. The initial amplitude A_0 reduces according to the attenuation coefficient α, which increases with the frequency of the wave: high-frequency waves undergo greater attenuation as they interact more intensely with microscopic defects and internal bonds, with α proportional to f^n, where n usually varies between one and two depending on the characteristics of the concrete.

When a US wave propagates in concrete, it is scattered every time it encounters a discontinuity, causing some energy to deviate from the original direction and reducing the amplitude of the received signal. This effect is particularly pronounced for high-frequency waves, especially when the defects are similar in size to the wavelength, complicating the interpretation and localization of internal defects.

Micro-cracks and porosity in concrete trap dissipate energy, deflecting waves and increasing attenuation. The pores, having a much lower acoustic impedance than the cement paste and aggregates, cause strong reflections and energy losses.

The combination of the above effects weakens and distorts the signal, requiring appropriate frequencies to balance resolution (which increases with frequency) and penetration (which decreases with frequency).

Remark 2. *Non-linear analysis is essential for understanding US propagation in concrete, a heterogeneous material with internal structural discontinuities. It goes beyond classical linear models by addressing phenomena like attenuation, micro-cracks, porosity, and internal defects, which serve as early degradation indicators. Advanced models, such as the Hammerstein model, are employed to detect and quantify these non-linearities, enabling a detailed interpretation of wave-defect interactions. This approach integrates artificial intelligence techniques to enhance early damage diagnosis, providing a comprehensive view of concrete behavior under dynamic stresses and supporting advanced monitoring and self-healing technologies.*

5. Non-Linear Analysis

High-resolution and sensitivity techniques require analytical–numerical models that consider both linear and non-linear components [60]. In fact [61,62], non-linear behaviors can be associated with discontinuities within concrete, with effects due to the shift of the resonance frequency as the stress amplitude increases, generation of higher order harmonics, interaction between stress high intensity and irregularity, and sensitivity to non-linear propagating phenomena (sensitive indicators of the first onset of damage) [63–65]. Furthermore, these principles allow the development of tools that provide results comparable with the performance of specific analytical models which, due to their high computational complexity, do not lend themselves to technology transfer [66].

Among the most recent approaches, Hammerstein models provide global parameters on the onset of defects, which can also be exploited in the case of self-repairing concrete. However, if their performances appear promising, the data processing, often affected by uncertainties and/or inaccuracies, requires adequate AI-based treatments with a reduced computational load that are advantageous for real-time applications and for HW prototyping [67–72].

Currently, scientific research is taking its first steps along this line of research, to which the CAIUS Project will make its contribution through the practical experimentation of this integration for significant and very interesting developments [73–76].

6. US High-Resolution and Big Data Technologies

The improvement of high-resolution US transmission and reception technologies makes it possible to obtain increasingly detailed and precise data with a consequent explosion in the amount of data collected, requiring the management and analysis of large volumes of information (big data).

They use frequencies higher than conventional ones, usually in the MHz range, detecting minute details in the internal structures of a material with a high spatial resolution.

Mathematically, the resolution is directly proportional to the frequency of the US signal $\Delta x = \frac{v}{2f}$, where Δx is the spatial resolution, v is the speed of sound in the material (which can be either v_P or v_s) and f is the frequency of the US signal. Increasing f reduces Δx, improving resolution and allowing you to distinguish more minor details within the material. But since $v_S < v_P$, S waves provide better spatial resolution than P waves and a slower velocity reduces the corresponding Δx, allowing more minor details to be distinguished. However, P waves are generally more used in US applications because they are less attenuated and can travel through more materials than S waves.

Remark 3. *This review focuses exclusively on supervised AI techniques, which are ideal for analyzing data from high-resolution US methods. By using labeled datasets with known defects, supervised models enable effective training and achieve high performance in detecting, localizing, classifying, and tracking damage evolution. Additionally, supervised approaches allow for continuous validation against known data, ensuring result reliability. In contrast, unsupervised techniques, which rely on*

large unlabeled datasets, need more precise references, making it harder to verify result accuracy and increasing ambiguity in interpreting US data.

7. Supervised AI Techniques for Identification and Classification of Defects in Concrete Using US

7.1. Convolutional Neural Networks (CNNs) for Defect Identification

CNNs effectively analyze US signals and are suitable for creating an abacus of 2D maps representative of various defects, a key objective of the CAIUS project. The CNN structure includes convolutional layers that extract relevant features from the maps, using filters to scan the signal and identify local patterns, such as edges, textures, and distinctive shapes, which can be associated with defects. Each convolutional layer is followed by a pooling operation, which reduces the dimensionality of the data while maintaining crucial information to simplify and facilitate defect identification. The data then pass through fully connected layers, which combine the extracted features for a final classification. In addition to 2D maps, CNNs are also effectively suited for analyzing 1D US signals, identifying significant features to improve the representation of recurring patterns, and increasing performance accuracy. In the context of the CAIUS project, CNNs will allow the recognition and cataloging of the different types of defects in concrete, building a detailed library of 2D maps and 1D traces associated with each defect and improving the precision and reliability in the monitoring and diagnosing of concrete structures [77–96]. A 2D US map can be represented by a two-dimensional matrix $X \in \mathbb{R}^{m\times n}$, where m and n indicate the width and height of the map, respectively. CNNs apply a filter $W \in \mathbb{R}^{p\times q}$ to X by scrolling over the signal image and applying a weighted sum of the values covered by the filter at each position [77–79]:

$$S(i,j) = \sum_{u=0}^{p-1}\sum_{v=0}^{q-1} X(i+u, j+v)W(u,v), \quad S \in \mathbb{R}^{(m-p+1)\times(n-q+1)}. \tag{22}$$

In (22), $S(i,j)$ is the value obtained by convolution over (i,j), describing how the filter interprets the local characteristics of the signal. The filter coefficients at position (u,v) are represented as well. An activation map, S, is thus obtained, highlighting the relevant characteristics of the portion of the signal on which the filter has been applied. The use of multiple filters, indicated with k, allows for obtaining different "feature maps", each of which highlights distinct aspects of the signal, $S_k \in \mathbb{R}^{(m-p+1)\times(n-q+1)\times k}$, where k is the number of filters used. Each feature map S_k captures specific information about the signal, such as edges, reflection patterns, and intensity variations that can indicate the presence of structural defects, such as micro-cracks or inclusions.

Remark 4. *CNNs automate the search for complex patterns in data, reducing the need for manual preprocessing. By applying multiple filters, CNNs can automatically identify relevant features of US signals that indicate the presence of defects. Furthermore, they build a representation library (feature maps) of the different types of defects that are functional for continuous monitoring, allowing the model to learn a wide range of concrete behaviors via the US signals and improving diagnosis capacity compared to traditional methods.*

Padding in a CNN adds pixels, usually of zero value, around the edges of an image before applying convolution to preserve the size of the output relative to the input, preventing the image from shrinking after each convolution. Without padding, the output tends to be smaller than the input, losing information at the edges (i.e., padding allows the size of the maps to be maintained during convolution operations). By applying a padding of p, (22) becomes the following [80–82]

$$S(i,j) = \sum_{u=0}^{p-1}\sum_{v=0}^{q-1} X(i+u-p, j+v-p)W(u,v). \tag{23}$$

The stride s in a CNN indicates how much the filter (or kernel) moves at each step during the convolution operation on a map. As the filter slides across the image, if the stride is one, the filter moves one pixel at a time, examining each subsequent position without skipping any. This means that the output will be larger as the convolution is computed in more detail. If the stride exceeds one (for example, two), the filter moves two pixels at a time, so it processes fewer positions in the image, producing a smaller output (resolution modulation). With s, the convolution is performed on multiple filter positions so that (23) becomes the following [83,84]:

$$S(i,j) = \sum_{u=0}^{p-1} \sum_{v=0}^{q-1} X(i+us, j+vs) W(u,v) \tag{24}$$

To identify and classify defects, the use of the ReLU activation function is particularly advantageous because it introduces non-linearity into CNN models, while maintaining low complexity. Operationally, the ReLU is applied element by element on the feature maps obtained from the convolution [85–87]:

$$S'_k(i,j) = \text{ReLU}(S_k(i,j)) = \max(0, S_k(i,j)), \tag{25}$$

which sets all negative values of $S_k(i,j)$ to 0, keeping only the positive ones unchanged, making only the learning of features that positively contribute to defect detection by eliminating noise effective. Furthermore, following [88,89],

$$\frac{\partial \text{ReLU}(x)}{\partial x} = \begin{cases} 1, & \text{se } x > 0, \\ 0, & \text{se } x \leq 0, \end{cases} \tag{26}$$

ReLU accelerates the network training process compared to activation functions such as the sigmoid or the hyperbolic tangent, affected by vanishing gradients.

By reducing the dimensionality of the feature maps S'_k and preserving the most relevant features, it selects the maximum value within a local window of size $r \times r$ [90]:

$$P(i,j) = \max_{(u,v) \in \text{pool window}} S'_k(i+u, j+v), \tag{27}$$

where poolwindow is the window of size $r \times r$ centered at (i,j) withinS'_k. This reduces the size of the output, producing more compact activation maps, $P_k \in \mathbb{R}^{\frac{m}{r} \times \frac{n}{r} \times k}$, where m and n represent the width and height of the original feature map, respectively, and k is the total number of filters applied during the convolution.

Remark 5. *Max pooling, a downsampling operation, reduces the computational load by lowering the feature map's spatial resolution while preserving the US signal's key characteristics. This enhances efficiency, prevents overfitting, and highlights local features of greater intensity, which correspond to reflections from internal discontinuities in the concrete, indicative of structural defects. Additionally, max pooling reduces local variance within pooling windows, improving the model's robustness to minimal signal variations such as noise or slight changes in reflectance.*

The resulting feature maps are flattened into an input vector $F = [f_1, f_2, \ldots, f_d]^T$ for the fully connected layer, where d is the total number of values resulting from the feature maps after pooling operations. Furthermore, f_i represents each value extracted from the feature maps reduced by pooling. This flattening process transforms the 2D feature maps into a linear format, allowing the network to consider all features extracted from the convolutions as a set of attributes representing the US signal.

The FLC computes a linear combination of these features using a weight matrix W_{fc} and a bias vector b, producing the output z of the fully connected layer, $z = W_{fc} \cdot F + b$. Furthermore, $W_{fc} \in \mathbb{R}^{l \times d}$ is the weight matrix that connects F to the l output neurons

(identifying the number of classes or output categories), while $b \in \mathbb{R}^l$ is the vector of biases associated with each output neuron.

This operation allows you to map the features learned in the previous layers of the network into a classification space, where each neuron represents a possible class of structural defect [91,92]. z is transformed through a softmax activation function, which converts z_i into probability, $\text{softmax}(z_i) = \frac{e^{z_i}}{\sum_{j=1}^{l} e^{z_j}}$, $\forall i = 1, \ldots, l$, where z_i is the score associated with the i-th class; $\text{softmax}(z_i)$ is the predicted probability for the i-th class and l is the number of total classes (defect types). softmax assigns each class a probability between 0 and 1, ensuring that the sum of the probabilities is equal to 1, allowing the model to express its confidence regarding which class the defect is present in, facilitating the classification of defects [91,92].

For training, a possible choice of cost function to minimize is cross-entropy, which measures the discrepancy between the distribution of predicted probabilities $\hat{y}$ and the real labels y, using $L = -\sum_{i=1}^{l} y_i \log(\hat{y}_i)$, where L represents the loss; $y_i \in \{0, 1\}$ is the real label for the i (one-hot encoded) class, with $y_i = 1$ only for the correct class and where $\hat{y}_i = \text{softmax}(z_i)$ is the probability predicted by the network for the class i. Cross-entropy strongly penalizes incorrect predictions, as it increases when the network assigns a low probability to the correct class. This helps the network better learn the differences between the ultrasonic signals associated with various defects [91,92]. This approach computes the gradients of L regarding the weights of the network and updates the weights by reducing the error by the following [93]:

$$\frac{\partial L}{\partial W_{fc}} = \frac{\partial L}{\partial z} \cdot \frac{\partial z}{\partial W_{fc}} = (\hat{y} - y) \cdot F^T, \tag{28}$$

where $\frac{\partial L}{\partial W_{fc}}$ is the gradient of the cost function regarding the weights W_{fc}; $\hat{y}$ is the vector of predicted probabilities, while y is the vector of real labels and F is the input vector to the fully connected layer. The gradient for the convolutional weights W is calculated as follows [93]:

$$\frac{\partial L}{\partial W} = \sum_i \sum_j \frac{\partial L}{\partial S'(i,j)} \cdot \frac{\partial S'(i,j)}{\partial W}, \tag{29}$$

where $\frac{\partial L}{\partial S'(i,j)}$ is the gradient of the loss regarding the output convolved at position (i, j), while $\frac{\partial S'(i,j)}{\partial W}$ is the gradient of the convolved output regarding the convolutional weights. Backpropagation is performed iteratively for each network layer, updating the weights to minimize the cost function.

Optimization Using the Adam Procedure

The Adam algorithm is used to improve convergence during training for its adaptability to gradient variations, improving stability and convergence speed. Its ability to automatically adjust the update pace makes the model more robust in detecting and classifying defects. The algorithm is based on the following steps [92–96]:

1. Gradient calculation: $m_t = \beta_1 m_{t-1} + (1 - \beta_1) \nabla_W L$ and $v_t = \beta_2 v_{t-1} + (1 - \beta_2)(\nabla_W L)^2$ where m_t is the estimate of the first moment (average of the gradients) while v_t is the estimate of the second moment (variance of the gradients); furthermore, $\nabla_W L$ is the gradient of the cost function regarding the weights W, and β_1 and β_2 are the control parameters, usually set to 0.9 and 0.999;
2. Bias correction: $\hat{m}_t = \frac{m_t}{1-\beta_1^t}$ e $\hat{v}_t = \frac{v_t}{1-\beta_2^t}$ where $\hat{m}_t$ and $\hat{v}_t$ are the corrected versions of the estimates m_t and v_t, which compensate for the bias introduced by the initial estimates;
3. Weight update: $W^{t+1} = W^t - \eta \frac{\hat{m}_t}{\sqrt{\hat{v}_t} + \epsilon}$, where W^{t+1} is the updated value of the weights while η is the learning rate. Finally, ϵ is a small value to avoid division by zero, usually equal to 10^{-8}.

The analysis of 1D signals using CNNs represents a significant advancement, as it represents a refined evolution of 2D analysis methodologies. In practice, the acquired US signal is treated as a 1D vector, where each element represents the amplitude of the US signal at a given time instant, with n denoting the total number of time samples. The 1D convolution is applied using a filter $w \in \mathbb{R}^p$, which slides along the time dimension of the signal. This process mathematically describes how each signal segment is multiplied by the filter, and the resulting sum forms a new convoluted signal vector, highlighting rapid amplitude changes that can indicate structural defects. The ReLU introduces non-linearity, maintaining only the positive values of the processed signal and eliminating the negative anomalies irrelevant to the defect analysis.

Even in 1D, pooling reduces the dimensionality of the signal, consolidating data with more dominant characteristics (i.e., maximum peaks), minimizing noise, and improving the reliability of model predictions. Finally, as in 2D, the output is flattened and passed through fully connected layers, which integrate all the extracted features. Finally, softmax transforms the linear scores into probabilities, assigning each defect class a probability based on the characteristics of the analyzed signal.

We observe that moving from 2D to 1D, we lose the ability to analyze the spatial and temporal variations of the signal simultaneously. However, the time dimension is more critical for defect detection for US signals, so 1D analysis is compelling. Furthermore, adapting analysis methods from 2D to 1D requires special attention in selecting and optimizing filters and network structures to ensure that vital information is not lost during the convolution and pooling process. This adaptation of 2D to 1D methodologies represents a critical area of innovation in the field of concrete structure monitoring, enabling precise and timely analysis based on US data with potential applications beyond civil engineering. For a detailed and technical view of these transformations, including filter and neural network configuration examples, see Table A1.

Remark 6. *Signal decomposition techniques are crucial for segmenting the signal into frequency bands to effectively analyze large volumes of US signals and detect, classify, and predict concrete defects. This enables the extraction of key features like frequency, energy, and amplitude variations, along with coefficients such as kurtosis and skewness, which aid in identifying cracks or voids. When integrated with AI algorithms like CNNs and supervised machine learning, these techniques improve the diagnosis and prediction of concrete conditions, optimizing predictive maintenance decisions. The following sections present some of the most relevant approaches combining US analysis with AI.*

8. Wave Packet Transform (WPT) and Backpropagation Neural Networks (BPNNs) with Optimization via Genetic Algorithm (GA)

The Wave Packet Transform (WPT) is an extension of the discrete wavelet transform (DWT), which allows for a more detailed and flexible analysis of 2D and 1D signals. This technique enables isolating and analyzing frequency, energy, and amplitude variations, making it crucial for identifying structural defects.

DWT decomposes a signal using a mother wavelet, producing a hierarchical representation of its components at different resolutions. For a 1D signal $f(t)$, the DWT is defined through the application of a low-pass filter, h, and a high-pass filter, g, giving the discrete decomposition of a signal at a level j as follow [97,98];

$$c_n^j[k] = \sum_{l \in \mathbb{Z}} h[l - 2k] c^{j+1}[l], \quad d_n^j[k] = \sum_{l \in \mathbb{Z}} g[l - 2k] c^{j+1}[l], \tag{30}$$

where $c^{j+1}[l]$ are the approximation coefficients at the $j+1$ level while $c_n^j[k]$ and $d_n^j[k]$ are, respectively, the approximation and detail coefficients obtained at the j level. In the DWT, only $c_n^j[k]$ are further decomposed at each level, producing a representation that captures the low-frequency components in greater detail.

WPT generalizes this process by decomposing each level's approximation and detail coefficients, where all frequency bands are split evenly. The WPT for 1D signals is formulated as follows [97–99]:

$$d^j_{2n}[k] = \sum_{l\in\mathbb{Z}} h[l-2k]d^{j+1}_n[l], \quad d^j_{2n+1}[k] = \sum_{l\in\mathbb{Z}} g[l-2k]d^{j+1}_n[l], \tag{31}$$

where $d^{j+1}_n[l]$ are the data at level $j+1$ and band n, while $d^j_{2n}[k]$ and $d^j_{2n+1}[k]$ represent the low- and high-frequency components at the j level, respectively, allowing the entire frequency spectrum to be explored in detail of the signal.

In 2D signals, filters are used along both dimensions, obtaining a detailed representation of the spatial and frequency components of the signal. In particular [97–99],

$$d^j_{2n_1,2n_2}[k_1,k_2] = \sum_{l_1,l_2\in\mathbb{Z}} h[l_1-2k_1]h[l_2-2k_2]d^{j+1}_{n_1,n_2}[l_1,l_2], \tag{32}$$

$$d^j_{2n_1+1,2n_2}[k_1,k_2] = \sum_{l_1,l_2\in\mathbb{Z}} g[l_1-2k_1]h[l_2-2k_2]d^{j+1}_{n_1,n_2}[l_1,l_2], \tag{33}$$

$$d^j_{2n_1,2n_2+1}[k_1,k_2] = \sum_{l_1,l_2\in\mathbb{Z}} h[l_1-2k_1]g[l_2-2k_2]d^{j+1}_{n_1,n_2}[l_1,l_2], \tag{34}$$

$$d^j_{2n_1+1,2n_2+1}[k_1,k_2] = \sum_{l_1,l_2\in\mathbb{Z}} g[l_1-2k_1]g[l_2-2k_2]d^{j+1}_{n_1,n_2}[l_1,l_2]. \tag{35}$$

In these expressions, $d^{j+1}_{n_1,n_2}[l_1,l_2]$ represent the sequence of the WPT at level $j+1$ and bands n_1, n_2, while $d^j_{2n_1,2n_2}[k_1,k_2]$, $d^j_{2n_1+1,2n_2}[k_1,k_2]$, $d^j_{2n_1,2n_2+1}[k_1,k_2]$, and $d^j_{2n_1+1,2n_2+1}[k_1,k_2]$ represent the components decomposed into different frequency bands.

Shannon entropy can be used to optimize the choice of the wavelet basis since it evaluates the energy distribution of the WPT coefficients, measuring the amount of uncertainty associated with a distribution and identifying the coefficients containing most of the relevant information, especially on the signal portions with significant energy content. Unlike other entropies, Shannon's entropies balance the amount of information preserved and the simplicity of the representation, ensuring optimal selection of components for accurate analysis of signals. The Shannon entropy can be defined as $M(d) = -\sum_j P_j \log_2 P_j$, where $P_j = |d_j|^2\|d\|^{-2}$ represents the normalized probability of the coefficients d_j of the WPT, and $\|d\|^2$ is the total energy of the signal [100,101].

Feature Extraction and Normalization

Once the signal has been reconstructed with the coefficients selected using the Shannon entropy of the WPT, a set of significant characteristics, both traditional and modern, can be extracted for a detailed description and advanced analysis of the signal. Among these, it is possible to include the mean μ, which provides a measure of the centrality of a signal; the standard deviation, σ, which quantifies the dispersion of the signal values around the mean value (provides information on how much the signal values are distributed regarding the mean); the kurtosis coefficient (K), which measures the "tip" of the distribution of signal values compared to a normal distribution; the skewness coefficient (γ), which measures the symmetry of the distribution of signal values; the energy ratio (E), which represents the total power of the signal; the Tsallis entropy, a generalization of the Shannon entropy; the autocorrelation coefficient, ACF, which measures the correlation of the signal with itself at different time lags; the fractal dimension, D, which measures the complexity of the signal and the Teager–Kaiser Energy Operator, Ψ, which captures the instantaneous energy variations of the signal. Normalizing the extracted features ensures better convergence. For example, the Min–Max Normalization, $x_{\text{norm}} = \frac{x-\min(x)}{\max(x)-\min(x)}$, and the Z-score Normalization, which uses the mean and standard deviation, $x_{\text{norm}} = \frac{x-\mu}{\sigma}$, ensure that

features have homogeneous scales, making it easier to learn the neural network model and improving the speed and effectiveness of convergence during the training process. Integrating traditional and advanced features gives the model a richer view of the signal, increasing its ability to diagnose structural defects and improve infrastructure condition monitoring accurately. Table A2 details some essential features, while Table A3 highlights the pros and cons of each of them [97–102].

Backpropagation neural networks (BPNNs), a supervised learning model, localize and classify defects in US signals by handling non-linear and complex data. Their layered structure captures detailed features of US signals, distinguishing between those with and without structural defects. The backpropagation process optimizes network weights by minimizing errors between predicted and actual outputs, enabling effective adaptation to training data and improving the accuracy of anomaly classification. It comprises an input layer accepting the feature vectors $X = \{x_1, x_2, \ldots, x_n\}$ extracted from the US signals. Furthermore, a hidden layer, consisting of l nodes, preludes an output layer, which localizes and classifies defects by mapping features learned from US signals to specific defect types and locations. During the forward propagation phase, the network calculates the output of the hidden node y_j using a weighted combination of the inputs and a bias, passing the result through a non-linear activation function $f(x)$, usually sigmoidal (but, of course, other activation functions can be used) [101–103]:

$$y_j = f\left(\sum_{i=1}^{n} w_{ij} x_i + b_j\right) \tag{36}$$

where x_i is the value of the i-th input, while w_{ij} is the weight that connects the i-th input to the hidden node j-th. Furthermore, b_j represents the bias associated with the j-th hidden node. Finally, $f(x)$ is the activation function, which introduces the non-linearity needed to model complex relationships in the data.

The precision of BPNNs is evaluated using an error function E, usually in quadratic form such as mean square error (MSE), $E = \frac{1}{2}\sum_{k=1}^{m}(t_k - o_k)^2$, where m is the total number of outputs of the network, while t_k is the target for the k-th output; furthermore, o_k is the actual output for the k-th node. The error backpropagation updates the weights w_{ij} and biases b_j through gradient descent, minimizing overall error. The gradient of error regarding each weight w_{ij}, $\nabla w_{ij} = -\eta \frac{\partial E}{\partial w_{ij}}$, considers the rate of learning, η, which controls the speed of updating while $\frac{\partial E}{\partial w_{ij}}$ quantifies the variation of E regarding w_{ij}, which is obtainable via the following chain of derivatives: $\frac{\partial E}{\partial w_{ij}} = \frac{\partial E}{\partial o_k} \cdot \frac{\partial o_k}{\partial y_j} \cdot \frac{\partial y_j}{\partial w_{ij}}$, where each term represents the sensitivity of the error regarding the final output, passing through the various levels of the network and propagating the information error towards the previous nodes.

The BPNN, thus structured, identifies and classifies defects by analyzing the characteristics of the US signal (i.e., intensity variations, reflections, and attenuation) that occur in the presence of discontinuities. Due to the multilevel structure and constant update of the weights, the network distinguishes different defects and provides precise indications of their location [97,100,101,104].

To optimize the parameters of the BPNN, as well as the optimal choice of the number of hidden nodes (to balance predictive capacity and generalization of the model), GAs capable of carrying out the optimization without predefining an optimal structure and allowing the network a high adaptation, avoiding problems of underfitting or overfitting. Indeed, some nodes limit the network's ability to represent complex patterns in the data, while an excessive number leads to an unnecessary increase in computational complexity. Through GA, w_{ij}, b_j, and l are represented by a chromosome, each of which encodes a complete network configuration: if the encoding is binary, each parameter is described as a sequence of bits; if the encoding is real, each gene represents a continuous numerical value. l is included in the chromosome, allowing the GA to search for the ideal number of

hidden nodes that optimizes the generalization capacity of the network, thus adapting to the variability of US signals [97–105].

Further, each chromosome C is evaluated, specifying the configuration of the BPNN. A commonly used fitness function is the mean square error (MSE) [104,105]:

$$F(C) = -\frac{1}{N}\sum_{k=1}^{N}(t_k - o_k)^2 \tag{37}$$

where N is the number of validation samples, t_k is the target of the k-th sample, and o_k is the output of the network as a function of the configuration of C. This function selects the chromosomes (that is, the configurations) with the highest accuracy and therefore the most suitable number of hidden nodes l [104,105].

GA applies to three main operators once the fitness for each C is known. The first concerns chromosomes with higher fitness that are more likely to be selected, favoring BPNNs with high learning efficiency. The second two selected chromosomes, C_1 and C_2, are combined to produce a new chromosome, $C_{\text{child}} = \{c_1, \ldots, c_p, c'_{p+1}, \ldots, c_m\}$, with p as the crossover point, exploring new combinations of weights, biases, and number of hidden nodes. Finally, mutation introduces random variations while avoiding premature convergence. For binary chromosomes, the mutation reverses some bits. For real chromosomes, the non-uniform mutation changes the numerical values with a random term decreasing over time, allowing for a more accurate search, $c_i = c_i + \Delta t(c_{\max} - c_i)$, where Δt decreases over time and $c_{\max}$ is the maximum allowed for c_i [104,105].

Cross-validation is applied during optimization to ensure that the selected number of hidden nodes offers good generalization ability. The dataset is divided into k partitions, with $k-1$ partitions used for training and one for validation. This process is iterated k times, ensuring that the BPNN is tested on different dataset configurations, preventing overfitting. The GA-based optimization approach for l selection allows the network to adapt optimally to the characteristics of US signals, offering a balance between complexity and predictive ability [105].

The state of adhesion of the concrete covering is essential to guarantee the durability and safety of the entire structure, as it protects from potentially harmful external agents. If the adhesion between the concrete covering and the underlying layer is compromised, discontinuities, cracks, and detachments are created, which reduce the effectiveness of the protection and expose the structure to possible freeze–thaw cycles.

For this type of problem, the combined action of US, the Continuous Wavelet Transform (CWT), and the Hilbert transform (HT) come to our aid by analyzing the waves reflected by the coating and concrete, identifying adhesion problems early and intervening with strategies of targeted maintenance, thus ensuring the safety and longevity of the structures.

CWT transforms the signal in the time–frequency domain by [103–105]:

$$CWT(a,b) = \frac{1}{\sqrt{|a|}}\int_{-\infty}^{+\infty} x(t)\psi^*\left(\frac{t-b}{a}\right)dt \tag{38}$$

where $x(t)$ is the US signal; $\psi(t)$ is the mother wavelet used for the transform; a is the scaling factor (which controls the frequency resolution); b is the translation parameter (which represents the position in time); and $\psi^*(t)$ is the complex conjugate of the parent wavelet. (38) extracts information such as the instantaneous frequency, the reflected echo's magnitude, and the reflected waves' time of flight (TOF).

CWT is preferred for coating analysis as it continuously represents the signal, allowing analysis at multiple scales and capturing continuous frequency variations. This capability enables the detection of rapid transitions and local events, such as coating/concrete adhesion defects, with fine temporal resolution, identifying punctual transients and small localized detachments. Additionally, evaluating the integrity of the concrete lining requires combining the temporal and frequency analysis provided by the CWT with the phase

variation detection of the Hilbert transform, which identifies delamination through the instantaneous phase of the reflected waves.

HT calculates the instantaneous phase of reflected waves, highlighting phase changes that indicate delamination, while CWT offers detailed analysis in the time–frequency domain. Formally, HT converts a real signal $y(t)$ into a complex analytical signal, $z(t)$, of the form $z(t) = y(t) + iH(t)$, where $H(t)$, the HT of $y(t)$, is given by the following [104]:

$$H(t) = \frac{1}{\pi} \int_{-\infty}^{+\infty} \frac{y(\tau)}{t-\tau} d\tau \tag{39}$$

from which the instantaneous phase of $y(t)$ is easily obtained via $\phi_k = \arctan\left(\frac{H(t)}{y(t)}\right)$.

If the coating adheres, the waves reflected from the surface and the back maintain a similar phase (the coating/concrete interface transmits regular energy). When delamination occurs, a gap is created between the coating and the concrete, causing a phase reversal of the echo reflected from the back. The primary parameters for assessing coating adhesion include TOF, which denotes the time required for a wave to travel and is influenced by coating thickness and defects, and the CWT magnitude ratio, which quantifies the attenuation of the US signal. In an adherent coating, some energy is transmitted to the concrete, increasing attenuation. Conversely, in the case of delamination, the reflected energy is greater, leading to decreased attenuation. The phase difference between the reflected waves is also of great importance. A zero phase difference indicates adhesion, while a phase shift of 180° signals delamination [104,105]. TOF, CWT ratio, and phase difference calculated via HT can be used as input to a CNN, providing complementary information: the TOF measures thickness and discontinuity, the CWT ratio evaluates signal attenuation and energy transmission, and the phase detects delamination via phase inversions. The CNN leverages these parameters to automatically learn complex patterns, identifying subtle details that significantly improve the classification accuracy of adhered and delaminated coatings.

Furthermore, this approach allows for a rapid and efficient binary classification (adhered or delaminated) compared to traditional US inspection methods, which are often subject to subjective interpretations. The CNN, trained on a large dataset of reflected signals, can generalize to new data in real time, reducing evaluation times and minimizing the risk of interpretation errors.

Remark 7. *Multi-Scale Convolutional Bidirectional Memory Networks (MCBMNets) enhance ultrasonic signal analysis by combining spatial pattern extraction with multi-scale resolution and bidirectional memory through LSTM. This approach captures local features and temporal dependencies, optimizing the interpretation of complex signals. The multi-scale analysis identifies patterns at different resolutions, while bidirectional memory improves the distinction between adherent and delaminated coatings by analyzing temporal relationships.*

Usually, a "cross-entropy" loss function is used to minimize the following type [104]:

$$L = -\frac{1}{N} \sum_{i=1}^{N} \sum_{k=1}^{K} y_{i,k} \log(p_{i,k}) \tag{40}$$

where N is the total number of samples, K is the number of defect classes, $y_{i,k}$ represents the true label of the sample i for the class k, and $p_{i,k}$ is the predicted probability that the sample i belongs to the class k. It measures the discrepancy between correct classification and incorrect classification. The architecture of an MCBMNet comprises four main blocks: an input block, Multi-Scale Convolution block, Bidirectional LSTM (BiLSTM) block, and output block. The input block segments the US signals into fixed-length time windows, which are then passed to the convolution block. This block is designed to extract features on different time scales via 1D convolutions with kernels of various sizes, which is usually performed using $z(n) = x(n) * w(n) = \sum_{m=1}^{l} x(m) \cdot w(n-m)$, where $x(n)$ is the input

signal, $z(n)$ is the output after the convolution operation, $w(n)$ is the 1D convolution kernel of length l, and ast represents the convolution operation to extract global and local features, from which a ReLU is applied. Next, to reduce the dimensionality, a max-pooling approach is applied.

The second block captures long-term dependencies in both the forward and backward directions in the sequential data, as follows [104,105]:

- For forward propagation: $h_t^F = \sigma(W_x^F x_t + W_h^F h_{t-1}^F + b^F)$.
- For backward propagation: $h_t^B = \sigma(W_x^B x_t + W_h^B h_{t+1}^B + b^B)$.

Here, h_t^F and h_t^B represent the hidden states of the forward and backward propagations, respectively, W_x^F, W_h^F, W_x^B, and W_h^B are the weight matrices associated with forward and backward propagation, x_t is the input at a time t, and b^F and b^B are the biases of the respective networks. The forward and backward outputs are then combined via $h_t = h_t^F \oplus h_t^B$ where $\oplus$ represents the concatenation of the vectors.

Three main gates constitute the LSTM unit. In particular, the forget gate is given by the following [104,105]:

$$f_t = \sigma(W_f \cdot [h_{t-1}, x_t] + b_f), \tag{41}$$

while the input gate and output gate are performed, respectively, as

$$i_t = \sigma(W_i \cdot [h_{t-1}, x_t] + b_i), \quad o_t = \sigma(W_o \cdot [h_{t-1}, x_t] + b_o) \tag{42}$$

Then, indicating with $\circ$ the product element by element, the new state of the cell can be calculated as follows:

$$c_t = f_t \circ c_{t-1} + i_t \circ \tanh(W_c \cdot [h_{t-1}, x_t] + b_c) \tag{43}$$

Finally, the hidden state is updated as $h_t = o_t \circ \tanh(c_t)$. After the BiLSTM block, the output is passed to a Fully Connected Layer and then to a softmax function for classification. The model is optimized using Adam's algorithm.

Tables A4 and A5 present the SWOT analyses of the supervised AI techniques presented in this review for defect localization and classification.

Several supervised artificial intelligence techniques are used to detect defects in concrete using ultrasound. The BPNN-GA method is fast and efficient for identifying defects such as holes and cracks. Mask RCNNs, with high precision, detect cracks and delamination, facilitating automated structural monitoring. Based on the wavelet transform, the CW-HT-CNN model distinguishes the degradation of thin coatings and material adhesions. MCBMNet, thanks to the multi-scale network and the BiLSTM block, identifies cavities while resisting noise. Finally, WPT-SCNs excel in precisely recognizing penetrating cavities, outperforming traditional methods.

9. Supervised AI Techniques for Predicting Defects in Concrete Using US

DWT can be combined with CNNs to detect cracks in concrete, leveraging the strengths of both techniques to improve the accuracy of internal crack detection and monitoring.

The multiresolution analysis technique decomposes a US signal into multiple scales, allowing local signal characteristics, such as discontinuities and cracks, to be examined. Based on the concept of mother wavelet, $\psi(t)$ generates a family of wavelets through dilations and translations, allowing a detailed analysis of the internal structures of the signal. Formally, if a and b are scale parameters [103–105],

$$\psi_{a,b}(t) = \frac{1}{\sqrt{|a|}} \psi\left(\frac{t-b}{a}\right). \tag{44}$$

The DWT of a signal $x(t)$, defined as in (38), using the (44), in the context of defect prediction, is more suitable because the CWT for each scale and translation requires an infinite

quantity of coefficients. Then, the DWT, discretizing the scale and translation parameters, for example, with powers of 2, is widely used, obtaining the following [103–105]:

$$\psi_{j,k}(t) = 2^{\frac{j}{2}} \psi(2^j t - k) \tag{45}$$

where j is the scale index and k the translation index. Then, the DWT of $x(t)$ is then given by the following [103–105]:

$$d_X(j,k) = \int_{-\infty}^{+\infty} x(t) \cdot 2^{\frac{j}{2}} \psi(2^j t - k)\, dt, \tag{46}$$

where j is the scale index and k the translation index. The Fast Wavelet Transform (FWT) algorithm is often used to calculate the DWT, which is based on a cascade of low-pass and high-pass filtering followed by downsampling. In particular, the low-pass filter is given by the coefficients $h[n]$ associated with the mother wavelet, and the high-pass filter is given by the coefficients $g[n]$, derived from $h[n]$ through the relation $g[n] = (-1)^n h[1-n]$. At each step, the signals are filtered and downsampled by a factor of two, producing a multiresolution representation [103–105]:

$$A_{j+1}[n] = \sum_k A_j[k] \cdot h[2n-k], \quad D_{j+1}[n] = \sum_k A_j[k] \cdot g[2n-k] \tag{47}$$

The result of the DWT is a series of coefficients representing the signal at different resolutions. The set of these coefficients is used to create a scalogram, which is an image representation of the signal energies at different scales; $S_X(j,k) = |d_X(j,k)|^2$ is used, for example, as input to the CNN model.

Remark 8. *FWT and DWT are closely related, but they are different. DWT breaks down a signal into low- and high-frequency components using a pair of filters and operates on discrete signals, allowing multiresolution representation in the time–frequency domain. On the other hand, the FWT calculates the DWT by exploiting the recursive structure of the transform to reduce the computational complexity to $O(N)$, making the decomposition much faster than direct methods.*

Once the scalogram has been generated, it is provided as input to a convolutional neural network (CNN), which extracts relevant features from the scalogram images. This allows the identification and analysis of patterns associated with structural defects in concrete, such as the presence and evolution of cracks. Following convolution, a nonlinear activation function (e.g., the ReLU) and a pooling layer are applied, which reduces dimensionality while retaining the most meaningful information and reducing computational complexity. Recently, multiple convolutional-layer approaches followed by pooling layers have been developed to improve the model's ability to learn complex representations without incurring overfitting. The features extracted in the initial convolutional layers are more basic, such as edges and textures, while those in the deeper layers capture more complex patterns specific to structural defects that can indicate the progression of cracks over time (B1).

At the end of the CNN, an FCL is inserted that aggregates the detected information to provide a prediction of the condition of the concrete, indicating the presence and potential development of cracks. The prediction can be binary (presence or absence of cracks) or, using the softmax function, extended to categorize that indicate different stages of evolution of the defect. If z_1 and z_2 represent the logarithmic scores of the classes (e.g., initial crack and advanced crack), then the following holds [103–105]:

$$P(\text{initial crack}) = \frac{e^{z_1}}{e^{z_1} + e^{z_2}}, \quad P(\text{advanced crack}) = \frac{e^{z_2}}{e^{z_1} + e^{z_2}}. \tag{48}$$

Optimization and Loss Function

The CNN is trainable by minimizing the cross-entropy based loss function (already presented above) for binary or multi-class classification, specified as below [103–105]:

$$L = -[y \log(P(\text{initial crack})) + (1 - y) \log(P(\text{advanced crack}))] \tag{49}$$

where y represents the actual label, with $y = 1$ for advanced cracks and $y = 0$ for initial cracks. The optimization algorithm that can be used is stochastic gradient descent (SGD), which updates the weights while minimizing the global loss. It is worth observing that during training, the model learns to generalize from the labeled examples' characteristics, distinguishing between incipient defects and those that have already evolved. This means that once trained, it can predict the presence of structural defects in new ultrasonic signals (which it has never seen) and their possible development over time. This ability to anticipate the evolution of defects is fundamental for the predictive maintenance of concrete structures, allowing timely interventions to avoid critical deterioration.

Remark 9. *The approach combining DWT and CNN can be easily adapted to 1D US signals. DWT breaks down the signal into multiresolution components that allow both low- and high-frequency information to be analyzed, providing a detailed representation of the local characteristics of the signal. The CNN, through one-dimensional convolutions, automatically extracts the relevant patterns, reducing the complexity of the signal and providing an accurate prediction of the presence of cracks.*

It is a non-destructive technique for detecting internal defects in concrete, such as voids and microcracks, by analyzing compression and shear waves. Based on wave propagation and the acoustic properties of the material, it determines the frequency and speed of the waves, related to the presence of structural defects and the strength of the concrete.

With the IE method, v_P and v_S represent input variables for regression models that predict mechanical properties of concrete, such as the compressive strength f_c. The relationship between wave speed and concrete strength can be modeled by linear regression, $y = \beta_0 + \beta_1 x$ where y is the output, which can be f_c; x is the input variable, for example, v_P or v_S; β_0 is the intercept; and β_1 is the regression coefficient indicating the contribution of wave speed to drag.

To obtain β_0 and β_1, supervised linear regression is used by minimizing the MSE between the predicted values $\hat{y}_i$ and the observed ones y_i. The error function is defined as $E(\beta_0, \beta_1) = \frac{1}{N} \sum_{i=1}^{N} (y_i - (\beta_0 + \beta_1 x_i))^2$; its minimization allows us to obtain β_0 and β_1 [103–105],

$$\beta_1 = \frac{\sum_{i=1}^{N} (x_i - \bar{x})(y_i - \bar{y})}{\sum_{i=1}^{N} (x_i - \bar{x})^2}, \quad \beta_0 = \bar{y} - \beta_1 \bar{x} \tag{50}$$

where $\bar{x}$ and $\bar{y}$ are the average of x and y in the dataset, respectively. The coefficients β_0 and β_1 allow us to predict the resistance of the concrete as a function of the speed of the US waves. A positive β_1 indicates that an increase in wave speed (v_P or v_S) is associated with an increase in drag, providing a quantitative measure of the relationship between structural quality and non-linear measurements.

This technique trains an ANN to classify and predict defects with an optimization mechanism of weights, biases, and network structure based on the dynamics of imperial relations, where the imperialist (a dominant solution) influences the position of the colonies (subordinate solutions), allowing effective exploration of the solution space. The initial population consists of N candidate solutions, each representing a configuration of the ANN with specific weights, biases, and structural parameters. These solutions are divided into imperialists (the best solutions, which act as leaders) and colonies (subordinate solutions that gravitate around the imperialists). The overall population is then distributed across a number N_I of empires, each consisting of an imperialist and its colonies. Each colony approaches the associated imperialist following an assimilation

movement, which can be formulated as $x_c \leftarrow x_c + \gamma(x_i - x_c)$ where x_c is the position of the colony (current configuration of the subordinate solution), x_i is the position of the imperialist (the dominant reference solution), and γ is a positive parameter (typically between 0 and 1) that controls the assimilation intensity. This movement allows the colony to gradually approach the dominant solution, iteratively improving its configuration based on the most promising solution [104,105]. To avoid premature convergence and ensure good exploration, a revolution mechanism is applied, which introduces random variations in the positions of some colonies ($x_c \leftarrow x_c + \delta$), where δ explores new areas of the solution space. This allows you to escape from local minima and reduces the risk of blocking in suboptimal configurations.

Empires compete, and colonies may move to another imperialist if that proves superior. This aspect favors the selection of the most promising configurations, with the less effective empires gradually losing power and being absorbed by the better performing ones.

Remark 10. *ICA is ideal for predicting defects in concrete using US, as it effectively explores the parameter space of the ANN, balancing exploitation and exploration. With the ability to adapt to significant signal amplitude and frequency variations, ICA finds optimal configurations to detect complex defects. Furthermore, the revolution mechanism avoids locking in local minima, making it particularly suitable for complex, non-linear problems such as defect classification.*

The support vector machine (SVM), used to predict and classify defects in concrete using ultrasound, identifies a hyperplane that maximizes the margin between classes, effectively distinguishing between signals of intact material and those indicative of structural defects. The SVM distinguishes between two classes by looking for a hyperplane $w \cdot x + b = 0$ that maximizes the margin, i.e., the minimum distance between the plane and the samples of each class. w orients the hyperplane, x represents characteristics of the sample (such as amplitude and frequency), and b determines its position. Maximizing the margin ensures better generalization, reducing classification errors on new data [103–105]. The SVM solves the separation problem by maximizing the margin between classes and minimizing the vector's norm w. Formally, the problem is formulated as a constrained optimization problem: $\min_w \frac{1}{2}\|w\|^2$ subject to $\quad y_i(w \cdot x_i + b) \geq 1, \forall i$ where y_i is the class label of the i-th sample, which takes values $+1$ for a class and -1 for the other, x_i is the feature vector of the i-th sample, and $w \cdot x_i + b$ represents the decision function for the i-th sample. The condition $y_i(w \cdot x_i + b) \geq 1$ guarantees that the edge of the hyperplane correctly separates the samples of the two classes. By minimizing $\frac{1}{2}\|w\|^2$, the SVM optimizes the distance between classes, selecting the separation plane that maximizes the robustness of the classification [103–105].

In many practical cases, defects in concrete may belong to more than two categories, requiring multiclass classification capability. SVMs, born for binary problems, can be adapted to multiclass problems using approaches such as One-vs-One (OvO), in which a separate classifier is trained for each pair of classes. In the case of C classes, this approach creates $\frac{C(C-1)}{2}$ classifiers. Each pair provides a vote for classification, and the class with the most votes is assigned to the sample [103–105].

Remark 11. *SVMs are effective for predicting concrete defects because they can handle non-linear separations using kernels like radial or polynomial to achieve linear separability in higher-dimensional spaces. By maximizing the separation margin, SVMs improve reliability and reduce error probabilities on unseen data. Techniques like One-vs-One (OvO) enable SVMs to differentiate between various defect types, including microcracks, inclusions, and voids.*

SVR, deriving from SVMs, solves regression and prediction problems by finding a function $f(x)$, approximating input–output, and minimizing the error within a defined

tolerance margin (epsilon-insensitive loss). Consider the SVR function $f(x)$, which approximates the output y given a set of training data

$$\{(x_1, y_1), (x_2, y_2), \ldots, (x_n, y_n)\} \tag{51}$$

with $x_i \in \mathbb{R}^d$ (where d is the number of features) and $y_i \in \mathbb{R}$. The objective function in SVR is constructed to minimize a cost function that combines the loss of the training data with the regularization of the model weights to improve the generalization ability [103–105].

The regression function in the SVR is expressed as $f(x) = \langle w, x \rangle + b = w^T x + b$ where w is the weight vector, b is the bias, and $\langle \cdot, \cdot \rangle$ represents the dot product. The epsilon-insensitive loss function is introduced to penalize errors only when they exceed a certain threshold ϵ. For a single pair (x_i, y_i), the loss function takes the following form [103–105]:

$$L_\epsilon(y_i, f(x_i)) = \max(0, |y_i - f(x_i)| - \epsilon) \tag{52}$$

ignoring errors within the range $[-\epsilon, +\epsilon]$, while linearly penalizing those exceeding ϵ.

The objective of SVR is therefore to minimize the trade-off between model complexity and prediction error. The formulation of the optimization problem is as follows [103–105]:

$$\min_{w,b,\xi,\xi^*} \frac{1}{2}\|w\|^2 + C\sum_{i=1}^{n}(\xi_i + \xi_i^*) \tag{53}$$

subject to

$$\begin{cases} y_i - \langle w, x_i \rangle - b \leq \epsilon + \xi_i, \\ \langle w, x_i \rangle + b - y_i \leq \epsilon + \xi_i^*, \\ \xi_i, \xi_i^* \geq 0. \end{cases} \tag{54}$$

In (53), $\|w\|^2$ represents the norm of the weight vector, which we try to minimize to obtain a simpler model while C is a regularization parameter that balances the penalty of errors with the complexity of the model. Finally, ξ_i and ξ_i^* are slack variables introduced to allow prediction errors beyond the margin ϵ.

Using Lagrange multipliers, it is possible to rewrite the problem in a dual form [103–105]:

$$\max_{\alpha,\alpha^*} -\frac{1}{2}\sum_{i,j=1}^{n}(\alpha_i - \alpha_i^*)(\alpha_j - \alpha_j^*)\, langle x_i, x_j \rangle - \epsilon\sum_{i=1}^{n}(\alpha_i + \alpha_i^*) + \sum_{i=1}^{n} y_i(\alpha_i - \alpha_i^*) \tag{55}$$

subject to $\sum_{i=1}^{n}(\alpha_i - \alpha_i^*) = 0$ and $0 \leq \alpha_i, \alpha_i^* \leq C$. In this formulation, α_i and α_i^* are the Lagrange multipliers associated with the regression constraints. The final solution of the regression function will be expressed as a linear combination of the support points, i.e., those points for which α_i or α_i^* are non-zero, $f(x) = \sum_{i=1}^{n}(\alpha_i - \alpha_i^*)\langle x_i, x \rangle + b$. To handle non-linear problems, you can use a kernel function $K(x_i, x_j)$, which implicitly maps the data into a higher-dimensional space, allowing you to find a linear function in this space that corresponds to a non-linear function in the original space. The prediction function then becomes

$$f(x) = \sum_{i=1}^{n}(\alpha_i - \alpha_i^*)K(x_i, x) + b. \tag{56}$$

Some commonly used kernels include the following: Linear Kernel, $K(x_i, x_j) = \langle x_i, x_j \rangle$; Polynomial kernel, $K(x_i, x_j) = (\langle x_i, x_j \rangle + 1)^d$; Gaussian Kernel (RBF), $K(x_i, x_j) = \exp(-\gamma\|x_i - x_j\|^2)$; and Sigmoid Kernel, $K(x_i, x_j) = \tanh(\kappa\langle x_i, x_j \rangle + \theta)$.

The values of the multipliers α_i and α_i^* identify the support vectors, i.e., the data within or beyond the margin ϵ, and only these contribute to the final predictive function. Support vectors define the fault tolerance boundaries of the model. The C parameter balances the importance of prediction errors and the simplicity of the model: a high value of C emphasizes the errors, complicating the model. ϵ establishes the width of the

tolerance margin, where smaller values reduce the prediction error but may increase the risk of overfitting.

SVR is adequate for prediction problems that require good generalization and robust management of model complexity and error margins. Thanks to kernels, it is a versatile technique applicable to linear and non-linear problems, offering flexibility without excessively increasing computational complexity.

The Hybrid Boosted Trees Regressor (BTR) and ANN model for the prediction of defects in concrete via US represents an advanced model for monitoring and predicting structural defects in concrete using ultrasonic data, combining techniques to improve accuracy in detecting and classifying defects such as voids, corrosion, and spalling. BTR uses decision trees to slice US data based on thresholds on characteristics such as propagation velocity, amplitude, and signal frequency. Each tree reduces the predictive error by minimizing the quadratic residual error and models the non-linear relationship between signal characteristics and defects, improving the model's accuracy.

In BTR, boosting combines weak trees into a more robust model. Each new tree is trained to reduce the error of the previous ones, using the residuals (differences between observed and predicted values) as targets for subsequent predictions. The final prediction is obtained by summing the weighted contributions of each tree, $\hat{y}_i = \sum_{m=1}^{M} \alpha_m f_m(x_i)$, where M is the total number of trees, $f_m(x_i)$ is the predictor of the m-th tree for the sample i, α_m represents the weight associated with the m-th tree, determined based on the tree's ability to reduce the error. This incremental process allows the model to become increasingly precise, progressively reducing residual error and strengthening the model's ability to identify defects via ultrasonic data.

Here, each tree is built on the residuals of the previous model, allowing the prediction to be improved at each step. The derivative of the loss function regarding the current predictions is calculated as $r_i^{(m)} = -\left[\frac{\partial L(y_i, F(x_i))}{\partial F(x_i)}\right]_{F(x)=F_{m-1}(x)}$ where $r_i^{(m)}$ represents the residuals for the sample i at the m-th iteration, $L(y_i, F(x_i))$ is the loss function, with the mean square error (MSE) given by $L(y_i, F(x_i)) = \frac{1}{2}(y_i - F(x_i))^2$, and $F_{m-1}(x)$ is the prediction accumulated up to the previous iteration $m-1$. Each new tree is trained on the calculated residuals, improving accuracy and correcting errors made by previous models. Gradient boosting allows the model to fit the data accurately, reducing the distance between predictions and actual values [103–105].

They constitute the second component of the hybrid model, designed to refine the predictions of defects in concrete further. Each ANN comprises multiple layers of neurons that automatically learn the relationships between ultrasonic data (input) and structural defects (output). In an ANN, the prediction $\hat{y}$ for each neuron is obtained through a linear combination of the weighted inputs and a bias, followed by a non-linear activation function of the type (36). By minimizing a loss function, the ANN is trained with algorithms, often based on gradient descent.

The hybrid approach initially exploits BTR to model the relationships between ultrasonic characteristics (such as wave amplitude, frequency, and speed) and the probability of defects. Subsequently, the residuals or predictions obtained from the BTR are used as input to an ANN, which can learn more complex relationships in the data and refine the predictions further. The combination of BTR and ANNs offers several mathematical and practical advantages. First, BTR allows you to capture nonlinear patterns in ultrasonic measurements, common in signals associated with structural defects. Furthermore, the ANN can exploit the data already processed by the BTR to learn complex and hidden patterns, improving defect classification. Finally, combining techniques reduces the risk of overfitting, making the model capable of generalizing new ultrasonic data and guaranteeing reliable predictions.

Remark 12. *Deep Convolutional Neural Networks (DCNNs) are advanced tools for predicting defects in concrete via US signals. Unlike traditional neural networks, DCNNs automatically extract the most relevant features, detecting hidden patterns and complex details. Their layered*

structure progressively analyzes signals, identifying defects such as voids, cracks, and structural discontinuities. This architecture allows for accurate classification between normal and abnormal conditions, improving monitoring accuracy and contributing to the safety and durability of building structures.

Remark 13. *T-distributed Stochastic Neighbor Embedding (t-SNE) is a dimension reduction technique helpful in visualizing and analyzing complex data in low-dimensional spaces, particularly effective in predicting defects in concrete using ultrasonic signals. t-SNE graphically represents hidden patterns, facilitating identifying groups or separations between classes, such as sound signals and defective concrete. Applied to US data with many variables, t-SNE simplifies complexity, making relevant features visible for defect classification and supporting exploratory analysis to improve accuracy and understanding of anomaly detection.*

Several hybrid supervised AI approaches are used to predict and detect defects in concrete through ultrasonic testing. Multi-scale signal analysis allows for identifying invisible internal cracks in critical infrastructures by combining discrete wavelet transform with convolutional neural networks. Algorithms such as Impact Echo, competitive imperial approaches, and SVM effectively classify structural defects such as voids, corrosion, and delamination, demonstrating a strong correlation between ultrasonic wave parameters and concrete properties. Furthermore, the integration of wavelet transform, deep convolutional neural networks, and t-SNE enables automated diagnosis of damage caused by temperature changes thanks to the time–frequency representation of ultrasonic signals. The combination of artificial neural networks and regression models ultimately showed an accurate prediction of the compressive strength of concrete, using data on cement content, electrical resistivity, and ultrasonic velocity to evaluate the quality of the material. Table A7 summarizes the SWOT analysis of supervised AI techniques for data prediction, while Table A8 summarizes some of the main results that have emerged in the recent literature.

10. Hammerstein Model: Operation and Use in US Non-Destructive Diagnostics for Localization, Classification, and Evolution of Defects in Concrete

This is a technique that explores the efficient estimation of synthetic indicators to evaluate the quality of non-linear systems, such as concrete structures, using US signals for defect localization, classification, and prediction [106–108].

In general, the Hammerstein model describes a non-linear system composed of a non-linear block followed by a linear block, making it suitable for representing the response of concrete when structural defects are present.

Mathematically, the model is expressed as $y(t) = \sum_{k=1}^{N} h_k(t) \otimes x^k(t)$, where $y(t)$ is the system output; $h_k(t)$ is the linear response of the concrete associated with the k-th power of the input $x(t)$, and $\otimes$ denotes the convolution operation. $y(t)$ can be analyzed to identify the presence of cracks or inhomogeneities in the material. The nuclei $h_k(t)$ reflect how the material responds at different powers to the US signal, providing valuable information for localizing the location of defects [106–108].

To identify the parameters of the Hammerstein model, a current choice uses exponential US signals, $x(t) = \cos(\varphi(t))$, where the phase $\varphi(t)$ varies with time such that the instantaneous frequency $\omega(t)$ is $\omega(t) = \frac{d\varphi(t)}{dt}$. This type of signal allows the concrete response to be analyzed at a range of frequencies, allowing defects to be localized based on the non-linear response. The exponential nature of the swept signal refers to how the frequency changes, growing exponentially over time, $f(t) = f_{\min} e^{\beta t}$, where $f_{\min}$ is the starting frequency while the parameter β acts as a control of the growth speed [106–108].

The pulse compression (PuC) technique is used to filter the response and obtain a more precise representation of the harmonic contributions using $u(t) = y(t) \otimes \psi(t) = \sum_{k=1}^{N} g_k(t)$, where $\psi(t)$ is the matched filter, and $g_k(t)$ represents the harmonic components of the response. The functions $g_k(t)$ allow estimating the position of defects since the parameters' variations indicate discontinuities in the material [106–108].

It is possible to use indices such as total harmonic distortion (THD) [106–108]:

$$\mathrm{THD}(f_0) = \sqrt{\sum_{k=2}^{\infty}\left(\frac{R_k}{R}\right)^2}, \tag{57}$$

where R is the amplitude of the fundamental component and R_k is the amplitude of the k-th harmonic. High THD values may indicate the presence of significant cracks. Other useful indices include intermodulation distortion (IMD):

$$\mathrm{IMD}_{2f_2-f_1}(f) = \frac{|G_{2f_2-f_1}(2f_2 - f_1)|}{|G_{f_1}(f_1) + G_{f_2}(f_2)|} \times 100\%, \tag{58}$$

where $G_{2f_2-f_1}$ performs the Fourier transform of the intermodulation component. These indices allow for the classification of the type of defect because of the non-linear frequency response. In addition to localization and classification, the Hammerstein model and extracted parameters can be used to predict the evolution of defects over time.

The ability to extrapolate Hammerstein model parameters for different signal amplitudes is critical for predicting the evolution of a defect. The relationship between the amplitude input parameters R_α and R_β is given by $g_\beta(t) = [\mathbf{A}_c^{-1}]^T \mathbf{R}_c \mathbf{A}_c^T g_\alpha(t)$, where $\mathbf{R}_c$ is a diagonal matrix whose elements represent powers of the ratio between R_β and R_α. This relationship allows for predicting how a defect might manifest at higher stress levels or under different stress conditions. For example, a small defect not appearing at low amplitude levels could become significant with a higher-intensity signal [106–108].

The damage index "Harmonic Index" (HI), defined as $\mathrm{HI} = \frac{\sum_{k=2}^{N}\int (g_k(t))^2 dt}{int(g_1(t))^2 dt}$, can be used as a critical indicator to monitor damage progression. A significant increase in HI over time may indicate a progression of structural damage in the concrete, suggesting the need for immediate intervention [106–108].

Remark 14. *The identification technique presented in this article is based on the structure of the Hammerstein model, which is adequate for most applications but unsuitable for chaotic non-linear systems, as suggested by recent variants of this structure [109,110]. Additionally, the Hammerstein–Wiener model extends this approach by incorporating non-linearities at both the input and output stages, combined with a dynamic linear response. This advanced methodology accurately describes complex systems, such as materials subjected to ultrasonic waves, by capturing non-linear effects and temporal dynamics, making it ideal for monitoring and analyzing structural systems under varying conditions.*

Techniques based on the Hammerstein model are applied for detecting and classifying defects in concrete using ultrasonic methods, proving valid on both synthetic models and real samples. This approach allows the estimation of parameters starting from a single measurement and stands out for its robustness even in the presence of noise, making it suitable for non-destructive diagnostics. The use of the Hammerstein model, together with the pulse compression technique, has proven effective in detecting and distinguishing between linear and non-linear responses, being useful for precisely identifying cracks and microcracks. Finally, a recursive algorithm specific to Hammerstein models has been shown to achieve stable convergence with high accuracy and low complexity, as confirmed by tests on concrete mills, maintaining reliable performance even under noisy conditions and with different non-linearities. Table A9 presents the proposed procedures' SWOT analysis, while Table A10 highlights a significant summary of the most important results discussed above.

11. AI Techniques for Improving Hammerstein Model Performance

ANNs can be used to improve the non-linear modeling capabilities of the Hammerstein system, especially to optimize the non-linear part by improving the system's ability to handle US signals [111,112].

CNNs are particularly useful for processing US signals, as they are excellent at local pattern recognition. They can be used to extract relevant features from ultrasonic signals and improve defect classification.

RNNs can be used to improve defect prediction. Since US signals have temporal components, they can learn dependencies over time to improve their ability to predict future defects.

SVMs can be used to classify defects in ultrasonic signals. This approach is particularly effective when you have a dataset of labeled signals (i.e., with known defects) available. By integrating SVMs into the Hammerstein model, it is possible to improve the classification phase of the anomalies present in the signals [111,112].

Evolutionary optimization algorithms, such as GA or Particle Swarm Optimization (PSO), can be used to optimize the parameters of the Hammerstein model. These algorithms can find the optimal parameters for the non-linear component of the Hammerstein model, thus improving its ability to adapt to incoming ultrasonic signals.

A further extension can be the Hammerstein–Wiener model that combines non-linear components at the linear system's beginning and end. Artificial intelligence techniques can be used to optimize both non-linear components, for example, by using neural networks to model complex relationships in the data [111,112].

If labeled defect data exist, supervised learning techniques can be employed to build predictive models. For example, Random Forests (RFs) and Gradient Boosting (GB) can be employed for classification and defect prediction, improving the robustness of the Hammerstein model, which may not handle all ultrasonic signal dynamics effectively. Furthermore, deep learning techniques can be used to build more powerful non-linear regression models, improving defect prediction ability [113–115].

An innovative approach could be the integration of CNNs with Fourier transforms (FFTs), which allows ultrasonic signals to be transformed from the time domain to the frequency domain, simplifying the detection of defects.

Finally, preprocessing techniques such as WT or principal component analysis (PCA) can be used to reduce noise in the ultrasonic signals before feeding them into the Hammerstein model, thus improving the overall accuracy. Furthermore, data augmentation can help increase the number of signals available for training AI models. In Table A11, a couple of main results are reported regarding the use of the Hammerstein model for defect prediction. Furthermore, Table A12 presents three significant results relating to hybrid approaches exploiting the Hammerstein model and AI techniques [113–115].

Remark 15. *The integration of Hammerstein models with advanced fuzzy and neuro-fuzzy systems introduces a significant innovation in the structural monitoring of concrete by combining non-linear analysis with intelligent techniques. Hammerstein models detect non-linearities caused by internal defects, while fuzzy systems manage uncertainties, providing detailed interpretations of ultrasonic signals. Neuro-fuzzy systems enhance adaptability and transparency compared to neural networks, allowing continuous updates to address data variations and improve model clarity. Central to the CAIUS project, this approach focuses on early diagnosis and optimized predictive maintenance, offering a cost-effective and flexible alternative to solely relying on neural networks.*

12. CAIUS Project: Integration of Hammerstein Models and Fuzzy Neural Networks for Advanced Monitoring of Concrete Defects via US

The current scientific literature highlights a limited application of the synergy between the Hammerstein model and fuzzy logic-based AI techniques for defect monitoring in concrete using US. The CAIUS project aims to fill this gap by introducing an integrated approach that combines the Hammerstein model with fuzzy systems organized into advanced neuro-fuzzy networks. These networks use different types—types 1, 2, and 3 and intuitionistic—fuzzy logic to improve the accuracy and flexibility of monitoring.

Type 1 fuzzy logic is based on sets with fixed and determined membership values, where each element has a precise degree of membership, making it suitable for situations with less uncertainty. Type 2 fuzzy logic introduces additional flexibility by incorporating an uncertain membership function, allowing for modeling scenarios with greater variability and impreci-

sion in the data. Type 3 fuzzy logic extends this ability to manage further complexity, adapting to situations where uncertainty is even more complex and dynamic. Finally, intuitionistic fuzzy logic considers the degree of membership and non-membership and includes a degree of indeterminacy, making it particularly useful for representing high ambiguities.

In the latest generation of neuro-fuzzy systems, in which the fuzzy component can be type 1, 2, 3, or intuitionistic, the fuzzy logic approach is combined with the adaptive learning of neural networks. This allows the network to autonomously learn the fuzzy parameters and to dynamically adapt to changes in the data, improving the management of uncertainties. With these systems, the CAIUS approach will achieve more precise diagnosis and the ability to adapt to variable material conditions, making monitoring the propagation of defects in concrete more efficient and reliable.

Strengthened by what was expressed in the previous section, the CAIUS project aims to implement innovations in the localization, classification, and prediction of defects using US signals by integrating the Hammerstein model with type 1, 2, 3, and intuitionistic neuro-fuzzy networks. The use of type 1 neuro-fuzzy systems allows the characteristics of the signal, such as amplitude and frequency, to be transformed into linguistic terms, thus facilitating the identification, classification, and prediction of defects. Learning algorithms such as ANFIS optimize fuzzy rules, adapting them to the material to accurately detect microcracks and discontinuities even in noisy environments. Furthermore, type 2 neuro-fuzzy systems add flexibility in managing uncertainties, improving the accuracy of classification and localization in complex contexts, while type 3 neuro-fuzzy systems further enhance adaptability, addressing situations with high variability. Intuitionistic fuzzy logic also introduces the evaluation of belonging, non-belonging, and indeterminacy, providing a complete representation of the state of the material and allowing for a more in-depth analysis of defects.

This combination of approaches enables robust localization, precise classification, and reliable prediction of defects such as voids, cracks, and microcracks, ensuring effective preventive diagnosis to meet the monitoring objectives of the CAIUS project.

13. Conclusions

This review has highlighted significant scientific results in integrating advanced AI techniques with ultrasonic (US) methodologies for monitoring concrete structures, where high performance in signal processing and handling large volumes of data is required. Specifically, using the Hammerstein non-linear model, combined with neuro-fuzzy systems, has significantly enhanced the ability to diagnose, classify, and predict the evolution of internal defects. Additionally, the application of convolutional neural networks (CNNs) has automated the analysis of ultrasonic signals in both 2D and 1D, providing a fast and reliable method for detecting internal anomalies, even in the presence of noise or data distortions. Finally, the theory of poroelasticity has provided a robust physical foundation for understanding the propagation of ultrasonic waves in porous materials, paving the way for highly precise "Physics-Informed" models.

Future research directions include the development of more efficient algorithms for compressing and managing the large volumes of data generated by ultrasonic inspections, as well as adopting machine learning models capable of processing data in real-time with reduced computational overhead. Another critical challenge is the creation of standardized reference datasets that are representative of a wide range of operational conditions, aiming to improve the reliability and scalability of AI solutions. Furthermore, deeper integration between physical models and AI techniques could lead to more accurately describing concrete behavior under dynamic stresses.

Regarding engineering applications, these results offer advanced tools for predictive maintenance and continuous monitoring of critical infrastructure such as bridges, tunnels, dams, and civil buildings. The ability to generate detailed defect maps and automate diagnostic processes makes these methodologies particularly suited for timely and targeted interventions, reducing costs and enhancing structural safety. The proposed technologies

can extend infrastructure's service life, optimize repair processes, and support the transition toward more sustainable and resilient construction. The practical adoption of these solutions represents a tangible opportunity to improve civil infrastructure management and ensure higher safety standards.

Author Contributions: Conceptualization, G.A., P.B., M.R. and M.V.; methodology, G.A., P.B., M.R. and M.V.; validation, G.A., P.B., M.R. and M.V.; formal analysis, G.A., M.R., P.B. and M.V.; investigation, G.A., P.B., M.R. and M.V.; resources, G.A., P.B., M.R. and M.V.; data curation, G.A., P.B., M.R. and M.V.; writing—original draft preparation, G.A., P.B., M.R. and M.V.; writing—review and editing, G.A., P.B., M.R. and M.V.; visualization, G.A., P.B., M.R. and M.V.; supervision, G.A., P.B., M.R. and M.V.; project administration, G.A., P.B., M.R. and M.V.; funding acquisition, G.A., P.B., M.R. and M.V. All authors have read and agreed to the published version of the manuscript.

Funding: This research has been supported by the Italian Ministry of University and Research under the Program PRIN 2022: "Integration of Artificial Intelligence and Ultrasonic Techniques for Monitoring Control and Self-Repair of Civil Concrete Structures (CAIUS)"—Code 2022AZPLL8.

Data Availability Statement: Data are contained within the article.

Conflicts of Interest: The authors declare no conflicts of interest.

Abbreviations

The following abbreviations are used in this manuscript:

ACF	Autocorrelation Coefficient
AI	Artificial Intelligence
BilSTM	Bidirectional LSTM Block
BPNN	Backpropagation Neural Networks
BTR	Boosted Trees Regressor
CNN	Convolution Neural Network
CWT	Continuous Wavelet Transofrm
DCNN	Deep Convolutional Neural Network
DWT	Discrete Wavelet Transform
FCL	Fully Connected Layer
FWT	Fast Wavelet Transform
GA	Genetic Algorithm
HI	Harmonic Index
HT	Hilbert Transform
ICA	Imperialist Competitive Algorithm
IE	Impact Echo
LSTM	Long Short-Term Memory
MCBMNet	Multi-Scale Convolutional Bidirectional Memory Network
NDT	Non-Destrucive Testing
OvO	One-vs-One
PuC	Pulse Compression
ReLU	Rectified Linear Unit
SGD	Stochastic Gradient Descent
STM	Short Term Memory
SVM	Support Vector Machine
SVR	Support Vector Regression
TOF	Time of Flight
THD	Total Harmonic Distortion
t-SNE	T-distributed Stochastic Neighbor Embedding
US	Ultrasonics
DQT	Discrete Wavelet Transform
WPT	Wavelet Packet Transform

Appendix A

Table A1. Operations and functions of a 1D CNN, from convolution to weight optimization.

Convolutional Layer	signal x; $s(i) = \sum_{u=0}^{p-1} x(i+u)w(u), \quad s \in \mathbb{R}^{n-p+1}$, $s(i)$ is value convolved to position i; $x(i+u)$, US signal at position $i+u$; $w(u)$ filter value at position u; p, length of the filter; matrix X and filter W one-dimensional vectors.
ReLU and 1D Pooling	$s'_k(i) = \text{ReLU}(s_k(i)) = \max(0, s_k(i))$, $p(i) = \max_{0 \le u < r} s'_k(i+u)$, window $r \times r$ reduces to window of length r.
Fully Connected Layer	$f \in \mathbb{R}^d$, d total number of values after pooling operations, $f = [f_1, f_2, \ldots, f_d]^T$; weight matrix $W_{fc} \in \mathbb{R}^{l \times d}$; bias vector $b \in \mathbb{R}^l$; $z = W_{fc} \cdot f + b$, $z \in \mathbb{R}^l$ is output of layer, with l defect classes.
Activation and Classification Function	$\text{softmax}(z_i) = \frac{e^{z_i}}{\sum_{j=1}^{l} e^{z_j}}, \quad \forall i = 1, \ldots, l.$
Cost and Training Function	$L = -\sum_{i=1}^{l} y_i \log(\hat{y}_i)$, y_i real label (one-hot encoded); $\hat{y}_i$ probability predicted by softmax.
Backpropagation and Weight Update	$\frac{\partial L}{\partial W_{fc}} = (\hat{y} - y) \cdot f^T$, $\frac{\partial L}{\partial w} = \sum_i \frac{\partial L}{\partial s'(i)} \cdot \frac{\partial s'(i)}{\partial w}$, $\frac{\partial L}{\partial s'(i)}$ gradient of loss regarding output convolved at position i.
Optimization	as in Section 7.1.

Table A2. Features: formulations and characteristics.

Feature	**Characteristics**
$\mu = \frac{1}{N} \sum_{i=1}^{N} x(i)$	$x(i)$, signal values; N, total number of samples.
$\sigma = \sqrt{\frac{1}{N} \sum_{i=1}^{N} (x(i) - \mu)^2}$	$x(i)$, signal values; N, total number of samples; μ, mean of the signal.
$K = \frac{\frac{1}{N} \sum_{i=1}^{N} (x_i - \mu)^4}{\sigma^4}$	Values of K greater than 3 indicate a distribution with a longer tail (sharper) than a normal distribution, while values lower than this indicate a flatter distribution.
$\gamma = \frac{\frac{1}{N} \sum_{i=1}^{N} (x_i - \mu)^3}{\sigma^3}$	Positive values of γ indicate a skewed distribution with a longer tail towards the right, while negative values indicate a longer tail towards the left.
$E = \sum_{i=1}^{N} \lvert x_i \rvert^2$	This reflects the energy concentrated in the selected coefficients of the WPT, in line with the Shannon entropy analysis which favors the most informative coefficients.
$S_q = \frac{1 - \sum_{i=1}^{N} p_i^q}{q-1}$	here, q is a parameter that modulates the importance of the contributions. Tsallis entropy is useful for analyzing signals with non-Gaussian probability distributions, increasing sensitivity to signal structure.
$ACF(\tau) = \sum_{i=1}^{N-\tau} x_i \cdot x_{i+\tau}$	Here, τ is the lag. Autocorrelation provides information about the periodicity of the signal, helping to detect repetitive patterns.
$D = \lim_{\epsilon \to 0} \frac{\log(N(\epsilon))}{\log(1/\epsilon)}$	Here, $N(\epsilon)$ represents the number of boxes of size ϵ needed to cover the signal. The fractal dimension is useful for describing the roughness or complexity of the signal, and is especially useful in biological or environmental signals.
$\Psi(x_i) = x_i^2 - x_{i-1} \cdot x_{i+1}$	This measurement is sensitive to rapid changes in the signal, making it useful for detecting short-lived events such as transients.

Table A3. Pros and cons of different features extracted from signals.

Feature	Pros	Cos
μ	Provides a simple and intuitive measure of the central tendency of the signal.	Sensitive to outliers, which can distort the result.
σ	Measures the dispersion of data around the mean, useful for understanding signal variability.	Does not provide information about the shape of the distribution.
K	Detects the "peakedness" of the distribution, useful for identifying signals with high local variations.	Sensitive to extreme values, can be hard to interpret for non-Gaussian distributions.
γ	Indicates the symmetry of the distribution, useful for understanding if the distribution has a prevalent tail.	Does not provide information on the overall dispersion or variability of the signal.
E	Reflects the total power of the signal, essential for evaluating the presence of significant information.	Does not distinguish between different types of variations in the signal (e.g., transients versus steady components).
S_q	Provides a generalization of Shannon entropy, suitable for signals with non-Gaussian distributions.	Higher computational complexity than Shannon entropy, depending on the parameter q.
ACF	Useful for detecting periodicity and repeating signal patterns.	Requires a long time window to be meaningful, can be influenced by noise.
D	Measures the complexity and "roughness" of the signal, useful for analyzing biological or natural signals.	Complex to calculate, can be difficult to interpret physically.
Ψ	Sensitive to rapid changes in the signal, excellent for detecting transient events.	Can amplify noise in signals, requiring pre-filtering to be effective.

Table A4. SWOT analysis of supervised AI techniques for defect identification and classification.

	CNN	BPNN & GA	Mask RCNN
Strengths	CNNs offer high accuracy and precision in defect detection by learning complex patterns from ultrasound data. They automate detection, enhancing efficiency and enabling fast processing of large 2D and 1D datasets. Additionally, their adaptability and scalability make them suitable for various applications and configurations.	The GA optimizes the parameters of the BPNN, enabling faster and better solutions than a traditional BPNN. The BPNN handles complex non-linear problems well, such as detecting defects in non-homogeneous materials. With GA, greater accuracy and faster convergence are achieved compared to traditional methods.	Precise localization, distinguishing defects from noise and irrelevant details. Simultaneously performs defect classification with pixel-level segmentation, providing a detailed view of defective areas. Detects and segments various types of defects. Applicable on a large scale for automatic monitoring of extensive infrastructure.
Weaknesses	CNNs require significant computational resources and large labeled datasets, making data collection costly and time-consuming, especially for rare defects. They are prone to overfitting and may struggle to generalize to new data. Additionally, their implementation and optimization demand advanced expertise, limiting their use to specialists.	GA-BPNN requires substantial computational resources and long training times to find the optimum. While it converges faster than a traditional BPNN, GA optimization can be time-consuming, particularly with large datasets, and its performance heavily depends on complex parameter tuning.	Requires large datasets for training and high computational resources for inference. While the model performs well in many situations, it can be negatively affected by images with significant artifacts, reducing accuracy in such cases.
Opportunities	Advances in hardware and deep learning frameworks will make CNNs more efficient and accessible. Combining CNNs with other AI technologies could improve detection capabilities while increasing computational power, which enables real-time monitoring. The demand for predictive maintenance will create new opportunities for automated CNN-based systems.	The BPNN-GA approach can be applied to other predictive maintenance and defect detection areas, potentially automating concrete defect detection and reducing the need for human expertise. It can be combined with other AI technologies for improved accuracy and efficiency, and with advanced hardware, it could be used on portable devices for on-site applications.	Suitable for large-scale automated monitoring, especially where preventive maintenance is crucial. It can be integrated with robotic systems to reduce costs and applied in other sectors for defect segmentation in various materials, expanding its range of applications.

Table A4. *Cont.*

	CNN	BPNN & GA	Mask RCNN
Strengths Threats	X-ray tomography and Eddy Current tests may compete with CNNs combined with US. CNN models risk underperforming on different datasets or conditions, leading to false positives/negatives. High costs and strict regulations requiring validation and certification limit their large-scale adoption.	Advanced methods may outcompete BPNN-GA in accuracy and efficiency, while its complexity limits large-scale implementation. Evolving materials and real-world noise can reduce its effectiveness and require model adjustments.	Lighter deep learning models may offer better efficiency, but variability in conditions and data can impact performance if not adapted. The model may struggle to generalize to new or unexpected defects, reducing prediction reliability.

Table A5. SWOT analysis of supervised AI techniques for defect identification.

	CW-HT-CNN	MCBMNet	WPT-SCNs
Strengths	The integration of CWT, HT, and CNN enables precise diagnosis of the coating condition, detecting delaminations and critical defects, improving speed, and adapting to coatings of different thicknesses.	The architecture combines multi-scale feature extraction and a bidirectional model for robust representation of ultrasonic signals, optimizing memory with gates and accelerating training with Adam, ensuring precise defect classification with softmax.	It achieves over 90% accuracy in detecting defects in concrete, with better generalization than traditional models, fast computation, and no need for manual optimization. WPT enhances signal quality by filtering high-frequency noise.
Weaknesses	Implementing CWT, HT, and CNN is complex and time-consuming, especially with large datasets. The method is sensitive to noise in real environments and requires advanced technical skills and a large amount of training data.	MCBMNet requires significant computational resources, risks overfitting with limited datasets, and is difficult to interpret, with latency that can limit its use in rapid-response applications.	The approach requires a high computational load and may suffer from overfitting if the parameters are not balanced, restricting its use in resource-constrained environments.
Opportunities	The approach is suitable for non-destructive monitoring of various materials, optimizable with signal analysis, IoT, and advanced algorithms. It is ideal for early defect detection for safety-sensitive sectors, such as offshore, aerospace, and nuclear.	The architecture, adaptable to various time series, can become more efficient with optimization techniques and hardware advancements, enabling the use of MCBMNet on resource-limited devices. Larger datasets would improve robustness and reduce the risk of overfitting.	Extensible approach for detecting complex defects with accuracy and efficiency, making it suitable for structural monitoring. It could be enhanced by integrating deep learning techniques or more advanced networks to detect subtler defects.
Threats	Innovation in alternative methods and the rapid evolution of machine learning could reduce the use of ultrasound and require continuous updates. The method's complexity and environmental variations in offshore contexts limit its adoption.	Lighter models can offer similar performance with lower computational costs, but training data quality is crucial. The evolution of neural networks, such as Transformers, could render MCBMNet obsolete, and its complexity limits industrial adoption.	New AI approaches could outperform the proposed method on larger, more complex datasets. It faces implementation challenges in noisy environments, and its performance depends on the precise configuration of parameters.

Table A6. Hybrid supervised artificial intelligence approaches for defect detection in concrete using US techniques.

Ref.	Domain	Method	Conclusions
[77–80]	through-holes, cracks, foreign materials	BPNN-GA	Effectiveness of the approach in the automatic identification of defects in concrete, surpassing traditional systems in terms of accuracy and speed, making detection more efficient and independent of specialized skills.
[81–84]	cracks, delaminations	Mask RCNN	Mask RCNN is effective in detecting internal defects, demonstrating high accuracy and precision, outperforming models like YOLOv4 in defect segmentation. It is highly suitable for automated monitoring of concrete structures, reducing errors and speeding up the inspection process.
[85–89]	delamination and coating thinning	CW-HT-CNN	Local peaks of the CWT manually estimate the TOF of reflected echoes, useful for thin coatings. The attenuation of US energy is greater in adherent coatings than in delaminated ones, with clear phase differences. Automated classification.
[90–92]	dry and water-filled cavities	MCBMNet	Effective approach for detecting cavities in concrete, with over 98% accuracy. The multi-scale network and BiLSTM block enhance feature extraction and robustness, offering noise resistance and adaptability, surpassing traditional methods.
[93–96]	cavities, penetrating holes	WPT-SCNs	Effective approach for recognizing penetrating cavities, superior to traditional methods like BP networks with GA, achieving high accuracy.

Table A7. SWOT analysis of supervised AI techniques for data prediction.

	DWT and CNN	Impact Echo and ICA and SVM	BTR and ANN
Strengths	The approach offers high accuracy in detecting cracks without direct access, with CNNs for automation and wavelet-based multiresolution for early detection and timely monitoring.	Early and precise detection of internal defects with ICA and SVM, improving classification and structural quality assessment.	The hybrid approach of BTR and ANN enhances defect prediction accuracy and model robustness, reducing overfitting and error and adapting to various concrete conditions.
Weaknesses	Requires high computational power and a quality dataset to avoid overfitting and generalization issues, while noisy ultrasonic signals can reduce the accuracy of the CNN.	Using ICA and SVM requires specific expertise and high resources, with a risk of missing small or deep defects.	The combined use of BTR and ANN is computationally expensive, sensitive to data quality, and challenging to interpret.
Opportunities	The approach is suitable for monitoring complex structures, with potential improvements in efficiency and generalization through more powerful hardware and larger datasets.	The approach is adaptable to critical infrastructure and can be enhanced with complementary technologies, with opportunities for large-scale implementation due to increasing safety regulations.	The model is applicable in construction and civil engineering for structural monitoring and can be extended to materials other than concrete, improving efficiency and predictive maintenance through integration with artificial intelligence and IoT.
Threats	Environmental variations can reduce the accuracy of ultrasonic signals. Alternative technologies like X-rays, radar, or lasers may provide better results. High costs and the need for advanced hardware also limit large-scale adoption, especially for large infrastructure.	Competition with ultrasonic tomography, drones, and humidity and material variability can compromise results. Implementation requires significant resources and may face regulatory resistance, slowing practical application.	Alternative machine learning models could surpass this hybrid approach, while stricter regulations and technological changes could influence its application and slow its diffusion in the construction sector.

Table A8. Utilization of supervised hybrid AI approaches for defect prediction in concrete through ultrasonic testing.

Ref.	Domain	Method	Conclusions
[97,98]	Critical infrastructures, internal cracks.	DWT and CNN	An effective approach that achieved over 96% accuracy in detecting cracks in concrete and over 90% in prediction. Analyzing ultrasonic signals at different scales can also identify non-visible cracks. The CNN, trained with DWT data and the entire signal, reached an accuracy of 80% and is more suitable for complex applications than the FFNN.
[99,100]	Void, corrosion, delamination.	Impact Echo and competitive imperial algorithm and SVM	High accuracy in detecting and classifying defects, with significant correlations between ultrasonic wave parameters and concrete properties, demonstrating that the model can correctly predict the type of defect based on the collected data.
[101–103]	Voids, corrosion, detachment.	DWT and DCNN and t-SNE	Automated diagnosis of compression damage due to temperature variations uses the time-frequency spectrum of ultrasonic signals as input for pre-trained DCNN models. This method allows for damage identification with an accuracy of 98.2%
[104,105]	Voids, corrosion, detachment.	ANN and BTR	The CNN and BTR models demonstrated superior performance in predicting compressive strength, highlighting that combining cement content, electrical resistivity, and UPV allows a more accurate assessment of concrete quality.

Table A9. Hammerstein model: SWOT analysis.

Strengths	The Hammerstein model is ideal for describing the non-linear behaviors of concrete in the presence of cracks or voids, capturing distortions and variations in the signal caused by structural defects. The combination between the non-linear block, which represents the distortion, and the linear one, which describes the temporal dynamics, allows defects to be precisely localized and classified. By analyzing reflected ultrasonic responses and TOF together with harmonic distortions, hidden cracks or voids can be identified. Furthermore, the model monitors the evolution of defects, measuring periodic changes in harmonic components to detect the expansion of cracks or voids, enabling predictive maintenance. Indices such as liHI quantify the severity and evolution of the damage, preventing sudden structural failures.
Weaknesses	The accuracy of the Hammerstein model depends on the quality of the ultrasonic signal and the system's calibration. Noise, interference, and multiple reflections can compromise the accuracy of defect localization and classification. Although the model is adequate for simple defects such as cracks or voids, it has limitations in analyzing complex or multiple defects. Small defects or with poorly defined non-linear signals reduce the model's effectiveness. Furthermore, pattern identification is computationally intensive, requiring advanced software and computing resources that are not always available in the field.
Opportunities	Advances in ultrasound technologies, such as high-resolution transducers and advanced signal processing techniques, may improve the effectiveness of the Hammerstein model. The use of multi-element or phased array transducers increases the accuracy of defect location. Emerging technologies such as ultrasonic tomography can integrate with the model to obtain detailed 3D images. AI and machine learning can improve automatic defect classification. The Hammerstein model has great potential in NDT to monitor critical infrastructure, contributing to preventative maintenance and reducing the risk of catastrophic failure and repair costs.
Threats	Other non-destructive diagnostic methods, such as X-ray tomography, thermography, or vibration analysis, can compete with ultrasound and be more suitable for detecting internal defects or reflective materials. These methods may be preferred in some applications, reducing the use of the Hammerstein model. Furthermore, the ultrasonic method is sensitive to environmental conditions such as humidity, extreme temperatures, and heterogeneous materials, which can hinder the analysis. Implementing the model on large facilities or remote sites requires time and advanced equipment, posing a logistical challenge. Finally, slowly evolving defects may not show significant changes over short periods, limiting the model's effectiveness for short-term monitoring.

Table A10. Hammerstein approaches for defect detection in concrete using US techniques.

Ref.	Domain	Method	Conclusions
[106]	defect detection and classification	Hammerstein	The technique allows parameters to be estimated from a single measurement and has proven valid on synthetic models and real samples, detecting the increased nonlinearity caused by defects. The method is robust even in the presence of noise, making it useful for non-destructive diagnostics.
[107]	cracks and micro-cracks	Hammerstein	The paper proves that with the pulse compression technique, the Hammerstein model effectively and precisely detects defects in concrete, distinguishing linear and non-linear responses. The methodology proved to be valid on synthetic and real samples, robust even in noisy conditions, and suitable for non-destructive diagnostics.
[108]	defect classification	Hammerstein	The paper proposes a recursive algorithm for Hammerstein models, ensuring convergence to a stable minimum with high accuracy and low complexity. Tests on a cement mill confirm the effectiveness and reliability of the algorithm even in noisy conditions and with different nonlinearities.

Table A11. Hammerstein approaches for defect prediction in concrete using US techniques.

Ref.	Domain	Method	Conclusions
[111]	prediction	Hammerstein	The paper concludes that the Hammerstein model is effective for predicting the compressive strength of high-performance concrete, modeling nonlinear interactions between components and facilitating the identification of structural defects, thus improving material design and durability.
[112]	prediction	Hammerstein	Closed-loop control with defect monitoring, and continuous parameter adjustment, as well as the use of digital twins to optimize process quality and reliability.

Table A12. Hybrid hammerstein approaches for defect prediction in concrete using US techniques.

Ref.	Domain	Method	Conclusions
[113]	prediction	Hammerstein-Wiener & SVR	The Hammerstein–Wiener and SVR models effectively predict the compressive strength of jujube seed concrete. The HWM-M4 model stands out for its high precision, making it the most reliable in high accuracy applications.
[114]	prediction	Hammerstein & SVR	The research used ANN, SVR, and Hammerstein models to predict the mechanical properties of concrete with plastic waste and fly ash, finding that ANN outperforms SVR and Hammerstein in predictive accuracy, with up to 6% higher precision.
[115]	prediction	Hammerstein & PSO	Optimization with PSO to improve convergence in Hammerstein pattern identification. By dynamically changing the inertia weight, the PSO optimizes accuracy and identification time.

References

1. Feng, D.C.; Ding, J.Y.; Xie, S.C.; Li, Y.; Akiyama, M.; Lu, Y.; Beer, M.; Li, J. Climate Change Impacts on the Risk Assessment of Concrete Civil Infrastructures. *ASCE OPEN Multidiscip. J. Civ. Eng.* **2024**, *2*, 03124001. [CrossRef]
2. Rincon, L.F.; Moscoso, Y.M.; Hamami, A.E.A.; Matos, J.C.; Bastidas-Arteaga, E. Degradation Models and Maintenance Strategies for Reinforced Concrete Structures in Coastal Environments under Climate Change: A Review. *Buildings* **2024**, *14*, 562. [CrossRef]
3. Mishra, V.; Sadhu, A. Towards the Effect of Climate Change in Structural Loads of Urban Infrastructure: A Review. *Sustain. Cities Soc.* **2023**, *89*, 104352. [CrossRef]
4. Xu, G.; Zhao, J.; Chen, M.; Xu, L. Study on Flexural and Self-Repairing Properties of Shape Memory Alloy Concrete Beams. *Constr. Build. Mater.* **2024**, *443*, 137715. [CrossRef]
5. Lou, Y.; Wang, H.; Amin, M.N.; Arifeen, S.U.; Dodo, Y.; Althoey, F.; Deifalla, A.F. Predicting the Crack Repair Rate of Self-Healing Concrete Using Soft-Computing Tools. *Mater. Today Commun.* **2024**, *38*, 108043. [CrossRef]
6. Shaheen, N.;Khushnood, R.A.; Musarat, M.A.; Alaloul, W.S. Self-Healing Nano-Concrete for Futuristic Infrastructures: A Review. *Arab. J. Sci. Eng.* **2022**, *47*, 5365–5375. [CrossRef]
7. Damodhara Reddy, B.; Narasimha Reddy, P.; Aruna Jyothy, S.; Mohan Babu, M.; Venkata Kavyatheja, B. Predicting Compressive Strength of Self-Repairing Concrete Using Artificial Neural Networks. In *International Conference on Intelligent Manufacturing and Energy Sustainability*; Springer Nature: Singapore, 2023; pp. 495–504.
8. Silva, M. I.; Malitckii, E.; Santos, T.G.; Vilaça, P. Review of conventional and advanced non-destructive testing techniques for detection and characterization of small-scale defects. *Prog. Mater. Sci.* **2023**, *138*, 101155. [CrossRef]
9. Ramírez, I.S.; Márquez, F.P.G.; Papaelias, M. Review on additive manufacturing and non-destructive testing. *J. Manuf. Syst.* **2023**, *66*, 260–286. [CrossRef]
10. Zhao, X.; Zhao, Y.; Hu, S.; Wang, H.; Zhang, Y.; Ming, W. Progress in active infrared imaging for defect detection in the renewable and electronic industries. *Sensors* **2023**, *23*, 8780. [CrossRef]
11. Khedmatgozar Dolati, S.S.; Caluk, N.; Mehrabi, A. Non-destructive testing applications for steel bridges. *Appl. Sci.* **2021**, *11*, 9757. [CrossRef]
12. Santos, T.G.; Oliveira, J.P.; Machado, M.A.; Inácio, P.L.; Duarte, V.R.; Rodrigues, T.A.; Santos, R.A.; Simão, C.; Carvalho, M.; Martins, A.; et al. Reliability and NDT Methods. In *Additive Manufacturing Hybrid Processes for Composites Systems*; Springer: Cham, Switzerland, 2020; pp. 265–295.
13. Torbali, M.E.; Zolotas, A.; Avdelidis, N.P. A State-of-the-Art Review of Non-Destructive Testing Image Fusion and Critical Insights on the Inspection of Aerospace Composites Towards Sustainable Maintenance Repair Operations. *Appl. Sci.* **2023**, *13*, 2732. [CrossRef]
14. Sunil, P.; Chandu, P.; Vivek, D. A Review: Non-Destructive Testing (NDT) Techniques, Applications and FutureProspects. *J. Sci. Technol.* **2024**, *9*, 9–15. [CrossRef]
15. Fasasi, M.O. Enhancing Infrastructure Resilience with Non-Destructive Evaluation: GPR and IE Integration for Delamination Detection. *Adv. Eng. Des. Technol.* **2024**, *6*, 31–45.
16. Morabito, F.C., Versaci, M. A Fuzzy Neural Approach to Localizing Holes in Conducting Plates. *IEEE Trans. Magn.* **2001**, *37*, 3534–3537. [CrossRef]
17. Versaci, M. Fuzzy Approach and Eddy Currents NDT/NDE Devices in Industrial Applications. *Electron. Lett.* **2016**, *52*, 943–945. [CrossRef]
18. Versaci, M.; Angiulli, G.; Crucitti, P.; De Carlo, D.; Laganà, F.; Pellicanò, D.; Palumbo, A. A Fuzzy Similarity-Based Approach to Classify Numerically Simulated and Experimentally Detected Carbon Fiber-Reinforced Polymer Plate Defects. *Sensors* **2022**, *22*, 4232. [CrossRef]
19. Versaci, M.; La Foresta, F.; Morabito, F.C.; Angiulli, G. A fuzzy divergence approach for solving electrostatic identification problems for NDT applications. *Int. J. Appl. Electromagn. Mech.* **2018**, 57, 133–146. [CrossRef]

20. Versaci, M.; Angiulli, G.; La Foresta; F., Crucitti, P.; Laganá, F.; Pellicanó, D.; Palumbo, A. Innovative soft computing techniques for the evaluation of the mechanical stress state of steel plates. In *Applied Intelligence and Informatics, Proceedings of the Second International Conference, AII 2022, Reggio Calabria, Italy, 1–3 September 2022*; Springer: Cham, Switzerland, 2022; pp. 14–28.
21. Versaci, M.; Angiulli, G.; Di Barba, P.; Morabito, F.C. Joint Use of Eddy Current Imaging and Fuzzy Similarities to Assess the Integrity of Steel Plates. *Open Phys.* **2020**, *18*, 230–240. [CrossRef]
22. Roach, D. Real Time Crack Detection Using Mountable Comparative Vacuum Monitoring Sensors. *Smart Struct. Syst.* **2009**, *5*, 317–328. [CrossRef]
23. Rossi, M.; Bournas, D. Structural Health Monitoring and Management of Cultural Heritage Structures: A State-of-the-Art Review. *Appl. Sci.* **2023**, *13*, 6450. [CrossRef]
24. Solla, M.; Maté-González, M.Á.; Blázquez, C.S.; Lagüela-López, S.; Nieto, I.M.Analysis of Structural Integrity Through the Combination of destructive Testing Techniques in Heritage Inspections: The study Case of San Segundo's Hermitage (Ávila, Spain). *J. Build. Eng.* **2024**, *89*, 109295. [CrossRef]
25. Cacciola, M.; Calcagno, S.; Megali, G.; Morabito, F.C.; Pellicano, D.; Versaci, M. FEA Design and Misfit Minimization for in-Depth Flaw Characterization in Metallic Plates with Eddy Current Nondestructive Testing. *IEEE Trans. Magn.* **2009**, *45*, 1506–1509. [CrossRef]
26. Cacciola, M.; Morabito, F.C.; Polimeni, D.; Versaci, M. Fuzzy Characterization of Flawed Metallic Plates with Eddy Current Tests. *Prog. Electromagn. Res.* **2007**, *72*, 241–252. [CrossRef]
27. Angiulli, G.; Calcagno, S.; De Carlo, D.; Laganá, F.; Versaci, M. Second-Order Parabolic Equation to Model, Analyze, and Forecast Thermal-Stress Distribution in Aircraft Plate Attack Wing–Fuselage. *Mathematics* **2020**, *8*, 6. [CrossRef]
28. Singla, R.; Sharma, S.; Sharma, S.K. Infrared Imaging for Detection of Defects in Concrete Structures. *IOP Conf. Ser. Mater. Sci. Eng.* **2024**, *1289*, 012064. [CrossRef]
29. Wang, Y.; Cui, J.; Deng, J.; Zhou, H.Experimental Study of Thermally Damaged Concrete under a Hygrothermal Environment by Using a Combined Infrared Thermal Imaging and Ultrasonic Pulse Velocity Method. *Materials* **2023**, *16*, 1040. [CrossRef]
30. Tran, Q.H. Passive and Active Infrared Thermography Techniques in Nondestructive Evaluation for Concrete Bridge. *AIP Conf. Proc.* **2021**, *2420*, 050008.
31. Cai, H.; Cheng, C.; Na, R.; Zhang, H.; Zhou, J.; Jing, S.; Miao, C. Cooling-Excited Infrared Thermography for Enhancing the Detection of Concrete Filled Steel Tube Interfacial Debonding at Concrete Hydration. *Case Stud. Constr. Mater.* **2024**, *20*, e02995. [CrossRef]
32. Pozzer, S.; Omidi, Z.; El Refai, A.; López, F.; Ibarra-Castanedo, C.; Maldague, X. Passive Infrared Thermography for Subsurface Delamination Detection in Concrete Infrastructure: Capabilities. *Constr. Build. Mater.* **2024**, *419*, 135542. [CrossRef]
33. Morozova, N.; Shibano, K.; Shimamoto, Y.; Tayfur, S.; Alver, N.; Suzuki, T. Visualization and Evaluation of Concrete Damage in-Service Headworks by X-Ray CT and Non-Destructive Inspection Methods. *Front. Built Environ.* **2022**, *8*, 947759. [CrossRef]
34. Sidiq, A.; Gravina, R.J.; Setunge, S.; Giustozzi, F. High-Efficiency Techniques and Micro-Structural Parameters to Evaluate Concrete Self-Healing Using X-Ray Tomography and Mercury Intrusion Porosimetry: A review. *Constr. Build. Mater.* **2020**, *252*, 119030. [CrossRef]
35. Bernachy-Barbe, F.; Sayari, T.; Dewynter-Marty, V.; L'Hostis, V. Using X-Ray Microtomography to Study the Initiation of Chloride-Induced Reinforcement Corrosion in Cracked Concrete. *Constr. Build. Mater.* **2020**, *259*, 119574. [CrossRef]
36. Basu, S.; Thirumalaiselvi, A.; Sasmal, S.; Kundu, T. Nonlinear Ultrasonics-Based Technique for Monitoring Damage Progression in Reinforced Concrete Structured. *Ultrasonics* **2021**, *115*, 106472 [CrossRef] [PubMed]
37. Hafiz, A.; Schumacher, T.; Raad, A. A Self-Referencing Non-Destructive Test Method to Detect Damage in Reinforced Concrete Bridge Decks Using Nonlinear Vibration Response Characteristics. *Constr. Build. Mater.* **2022**, *318*, 125924. [CrossRef]
38. Caballol, D.; Raposo, Á.P.; Gil-Carrillo, F. Non-Destructive Testing of Concrete Layer Adhesion by means of Vibration Measurement. *Constr. Build. Mater.* **2024**, *411*, 134548. [CrossRef]
39. Vandecruys, E.; Martens, C.; Van Steen, C.; Nasser, H.; Lombaert, G.; Verstrynge, E. Preliminary Results on Acoustic Emission and Vibration-Based Monitoring of Locally Corroded Reinforced Concrete Beams. In Proceedings of the NDT-CE 2022—The International Symposium on Nondestructive Testing in Civil Engineering, Zurich, Switzerland, 16–18 August 2022; Volume 9.
40. Hajin, C; Popovics, J.S. NDE Application of Ultrasonic Tomography to a Full-Scale Concrete Structure. *IEEE Trans. Ultrason. Ferroelectr. Freq. Control* **2015**, *62*, 1076–1085.
41. Lorenzi, A.; Stein, K.; Reginatto, L.A.; Pinto da Silva Filho, L.C. Concrete Structures Monitoring Using Ultrasonic Tests. *Rev. Constr.* **2020**, *19*, 246–257. [CrossRef]
42. Ge, L.; Li, Q.; Wang, Z.; Li, Q.; Lu, C.; Dong, D.; Wang, H. High-Resolution Ultrasonic Imaging Technology for the Damage of Concrete Structures Based on Total Focusing Method. *Comput. Electr. Eng.* **2023**, *105*, 108526. [CrossRef]
43. Ashkar, M., et al. Application of Ultrasonic Models for Invesrigating the Properties of the Interface Between Roller Compacted Concrete (RCC) Layers. *NDT E Int.* **2021**, *124*, 102516. [CrossRef]
44. Zheng, Y.; Wang, S.; Zhang, P.; Xu, T.; Zhuo, J. Application of Nondestructive Testing Technology in Quality Evaluation of Plain Concrete and RC Structures in Bridge Engineering: A Review. *Buildings* **2022**, *12*, 843. [CrossRef]
45. Angiulli, G.; Calcagno, S.; La Foresta, F.; Versaci, M. Concrete Compressive Strength Prediction Using Combined Non-Destructive Methods: A Calibration Procedure Using Preexisting Conversion Models Based on Gaussian Process Regression. *J. Compos. Sci.* **2024**, *8*, 300. [CrossRef]

46. Burrascano, P.; Laureti, S.; Hutchins, D.; Ricci, M.; Senni, L. A Pulse Compression Procedure for the Measurement and Characterization of Non-Linear Systems Based on Exponential Chirp Signals. In Proceedings of the 2015 IEEE International Ultrasonics Symposium (IUS), Taipei, China, 21–24 October 2015; pp. 1–4.
47. Malfense Fierro, G.P.; Meo, M. Linear and Nonlinear Ultrasound Time Reversal Using a Condensing Raster Operation. *Mech. Syst. Signal Process.* **2022**, *168*, 107713.
48. Okazaki, S.; Iwase, H.; Nakagawa, H.; Yoshida, H.; Hinei, R. Effect of Moisture Distribution on Velocity and Waveform of Ultrasonic-Wave Propagation in Mortar. *Materials* **2021**, *14*, 790. [CrossRef] [PubMed]
49. Burrascano, P.; Callegari, S.; Montisci, A.; Ricci, M.; Versaci, M. (Eds.) *Ultrasonic Nondestructive Evaluation Systems: Industrial Application Issues*; Springer: Cham, Switzerland, 2015.
50. Versaci, M.; Calcagno, S.; Cacciola, M.; Morabito, F.C.; Palamara, I.; Pellicanò, D. Innovative Fuzzy Techniques for Characterizing Defects in Ultrasonic Nondestructive Evaluation. In *Ultrasonic Nondestructive Evaluation Systems: Industrial Application Issues*; Springer: Cham, Switzerland, 2015; pp. 201–232.
51. Lee, J.W.; Kim, J.S.; Hong, C.H.; Oh, T.M. Permeability Monitoring of Underground Concrete Structures Using Elastic Wave Characteristics with Modified Biot's Model. *Sci. Rep.* **2024**, *14*, 22110. [CrossRef]
52. Ohtsu, M.; Kunisue, F.; Nogami, K. BEM Analysis of Biot's Model for Dynamic Compaction of Concrete in Successive Placement. *Mater. Struct.* **2015**, *38*, 739-745. [CrossRef]
53. Meng, M.; Frash, L.P.; Carey, J.W.; Li, W.; Welch, N. Rapid Measurement of Biot Wffective Atress Xoefficient for Class-G Oil Well Cements. In Proceedings of the ARMA US Rock Mechanics/Geomechanics Symposium, Golden, CO, USA, 28 June–1 July 2020; p. ARMA-2020.
54. Ulm, F.J.; Constantinides, G.; Heukamp, F.H. Is concrete a Poromechanics Materials?—A Multiscale Investigation of Poroelastic Properties. *Mater. Struct.* **2004**, *37*, 43–58. [CrossRef]
55. Bai, P.; Shen, X.; Zhang, X.; Yang, X.; Yin, Q.; Liu, A. Influences of Compression Ratios on Sound Absorption Performance of Porous Nickel–Iron Alloy. *Metals* **2018**, *8*, 539. [CrossRef]
56. Xue, L.; Zhu, Z.; Weng, X.; Pan, R.; Shi, J. Estimation of the Transverse Wave Velocity in Siliceous Carbonate Reservoirs of the Dengying Formation in the Gaoshiti–Moxi Area, Sichuan Basin, China. *Energies* **2023**, *17*, 135. [CrossRef]
57. Jannelli, A. Adaptive Numerical Solutions of Time-Fractional Advection–Diffusion-Reaction Equations. *Commun. Nonlinear Sci. Numer. Simul.* **2022**, *105*, 106073. [CrossRef]
58. Chakraborty, J.; Katunin, A.; Klikowicz, P.; Salamak, M. Early Crack Detection of Reinforced Concrete Structure Using Embedded Sensors. *Sensors* **2019**, *19*, 3879. [CrossRef]
59. Laureti, S.; Ricci, M.; Mohamed, M.N.I.B.; Senni, L.; Davis, L.A.; Hutchins, D.A. Detection of Rebars in Concrete Using Advanced Ultrasonic Pulse Compression Techniques. *Ultrasonics* **2018**, *85*, 31–38. . [CrossRef] [PubMed]
60. Gaur, H.; Srivastav, A. A Novel Formulation of Material Nonlinear Analysis in Structural Mechanics. *Def. Technol.* **2021**, *17*, 36–49. [CrossRef]
61. Broda, D., et al. Modelling of Nonlinear Crack-Wave Interactions for Damage Detection Based on Ultrasound—A Review. *Sound Vib.* **2014**, *333*, 1097–1118. [CrossRef]
62. Burrascano, P.; Laureati, S.; Ricci, M. Harmonic Distorsion Estimate for Damage Detection. In Proceedings of the IEEE National Aerospace and Electronics Conference, Dayton, OH, USA, 23–26 July 2018; pp. 274–279.
63. Burrascano, P.; Di Bella, A.; Gliozzi, A.; Laureti, S.; Ricci, M.; Rizwan, M.K.; Scalerandi, M.; Tortello, M. A Comparison of Scaling Subtraction and Pulse Compression Methods for the Analysis of Elastic Nonlinearity. *Proc. Meet. Acoust.* **2019**, *38*, 065013.
64. Mevissen, F.; Meo, M. Nonlinear Ultrasound Crack Detection with Multi-Frequency Exitation—A Comparison. *Sensors* **2021**, *21*, 5368. [CrossRef]
65. Castellano, A.; Fraddosio, A.; Piccioni, M.D.; Kundu, T. Linear and Nonlinear Ultrasonic Techniques for Monitoring Stress-Induced Damage in Concrete. *ASME J. Nondestruct. Eval.* **2021**, *4*, 041001. [CrossRef]
66. Zhang, Z.; Li, S.; Wuin, X. Research onthe Behavior and Mechanism of Three-Dimensional Crack Growth Under Uniaxial Loading. *Adv. Mater. Sci. Eng.* **2021**, *2021*, 5560253. [CrossRef]
67. Kwon, H.; Joh, C.; Chin, W.J. 3D Internal Visualization of Concrete Structure Using Multifaceted Data for Ultrasonic Array pulse-echo Tomography. *Sensors* **2021**, *21*, 6681. [CrossRef]
68. de Lima Seiffert, H.L.; Balbo, J.T. Development and Validation of an Ultrasound Imaging Software for Nondestructive Evaluation of Concrete Pavement. *Rev. IBRACON Estrut. Mater.* **2021**, *14*, *e14511.* [CrossRef]
69. Zhan, H.; Jiang, H; Jiang, R. Three-Dimensional Images Generated from Diffuse Ultrasound Wave: Detections of Multiple Cracks in Concrete Structures. *Struct. Health Monit.* **2022**, 157922. [CrossRef]
70. Ngo, L.T.Q.; Wang, Y.R.; Chen, Y.M. Applying Adaptive Neural Fuzzy Inference Systems to Improve Concrete Strength Estimation in Ultrasonic Pulse Velocity Test. *Adv. Civ. Eng.* **2018**, *2018*, 2451915 [CrossRef]
71. Juncai, X.; Jingkui, Z.; Zhenzhong, S. Recognition Method of Internal Concrete Structure Defects Based on D-CNN. *J. Intelligente Fuzzy Syst.* **2022**, *11*, 22–29.
72. Panagiotis, G.; Skentou, A.D.; Bardhan, A.; Samui, P.; Lourenço, P.B. Soft Computing Techniques for Prediction of Concrete Compressive Strength Using Non-Destructive Tests. *Constr. Build. Mater.* **2021**, *303*, 124450.
73. Silva, F.A.N.; Delgado, J.M.P.Q.; Cavalcanti, R.S.; Azevedo, A.C.; Guimarães, A.S.; Lima, A.G.B. Use of Nondestructive Testing of Ultrasound and Artificial Neural Networks to Estimate Compressive Strength of Concrete. *Buildings* **2021**, *11*, 44. [CrossRef]

74. Chun, P.; Ujike, I.; Mishima, K.; Kusumoto, M.; Okazaki, S. Random Forest-Based Evaluation Techniques for Internal Damage in Reinforced Concrete Featuring Multiple Nondestructive Testing Results. *Constr. Build. Mater.* **2020**, *253*, 119238. [CrossRef]
75. Epple, N.; Fontoura Barroso, D.; Niederleithinger, E. Towards Monitoring of Concrete Structures with Embedded Ultrasound Sensors and Coda Waves—First Results of DFG for CoDA. In *Lecture Notes in Civil Engineering*; Springer International Publishing: Cham, Switzerland, 2021.
76. Shrifan, N.H.; Akbar, M.F.; Isa, N. Prospect of Using Artificial Intelligence for Microwave Nondestructive Testing TEchhnique: A Review. *IEEE Access* **2019**, *7*, 110628–110650. [CrossRef]
77. Hu, T.; Zhao, J.; Zheng, R.; Wang, P.; Li, X.; Zhang, Q. Ultrasonic Based Concrete Defects Identification via Wavelet Packet Transform and GA-BP Neural Network. *PeerJ Comput. Sci.* **2021**, *7*, 635. [CrossRef]
78. Zhang, Y.; Aslani, F.; Lehane, B. Compressive Strength of Rubberized Concrete: Regression and GA-BPNN Approaches Using Ultrasonic Pulse Velocity. *Constr. Build. Mater.* **2021**, *307*, 124951. [CrossRef]
79. Zhang, Y.; Aslani, F. Compressive Strength Prediction Models of Lightweight Aggregate Concretes using Ultrasonic Pulse Velocity. *Constr. Build. Mater.* **2021**, *292*, 123419. [CrossRef]
80. Hou, R.; Hou, Q. Prediction of the Shear Capacity of Ultrahigh-Performance Concrete Beams Using Neural Network and Genetic Algorithm. *Sci. Rep.* **2023**, *13*, 2145. [CrossRef]
81. Kuchipudi, S.T.; Ghosh, D. Automated Detection and Segmentation of Internal Defects in Reinforced Concrete Using Deep Learning on Ultrasonic Images. *Constr. Build. Mater.* **2024**, *411*, 134491. [CrossRef]
82. Tan, C.; Uddin, N.; Mohammed, Y.M. Deep Learning-Based Crack Detection Using Mask R-CNN Technique. In Proceedings of the 9th International Conference on Structural Health Monitoring of Intelligent Infrastructure, St. Louis, MO, USA, 4–7 August 2019; pp. 15–20.
83. Yuan, C.; Xiong, B.; Li, X.; Sang, X.; Kong, Q. A Novel Iintelligent Inspection Robot With Deep Stereo Vision for Three-Dimensional Concrete Damage Detection and Quantification. *Struct. Health Monit.* **2022**, *21*, 788–802. [CrossRef]
84. Gepiga, C.S.; Magana, P.; Sandoval, G.A.D.; Angelia, R.E. Automated Crack Detection and Measurement Based on Mask R-CNN and Image Analysis with Mobile Application. In Proceedings of the 5th International Conference on Electronics and Electrical Engineering Technology (EEET), Beijing, China, 2–4 December 2022; pp. 14–22.
85. Malikov, A.K.U.; Kim, Y.H.; Yi, J.H.; Kim, J.; Zhang, J.; Cho, Y. Neural-Network-Based Ultrasonic Inspection of Offshore Coated Concrete Specimens. *Coatings* **2022**, *12*, 773. [CrossRef]
86. Zhao, J.; Hu, T.; Zhang, Q. A Wavelet Packet Transform and Convolutional Neural Network Method Based Ultrasonic Detection Signals Recognition of Concrete. *Sensors* **2022**, *22*, 3863. [CrossRef]
87. Yang, H.; Shu, J.; Li, S.; Duan, Y. Ultrasonic Array Tomography-Oriented Subsurface Crack Recognition and Cross-Section Image Reconstruction of Reinforced Concrete Structure using Deep Neural Networks. *J. Build. Eng.* **2024**, *82*, 108219. [CrossRef]
88. Ye, J.; Toyama, N. Automatic Defect Detection for Ultrasonic Wave Propagation imaging Method Using Spatio-Temporal Convolution Neural Networks. *Struct. Health Monit.* **2022**, *21*, 2750–2767. [CrossRef]
89. Wu, Y.; Wang, Y.; Li, D.; Zhang, J. Two-Step Detection of Concrete Internal Condition Using Array Ultrasound and Deep Learning. *NDT E Int.* **2023**, *139*, 102945. [CrossRef]
90. Liao, X.; Yan, Q.; Zhang, Y.; Zhong, H.; Qi, M.; Wang, C. An Innovative Deep Neural Network Coordinating with Percussion-Based Technique for Automatic Detection of Concrete cavity Defects. *Constr. Build. Mater.* **2023**, *400*, 132700. [CrossRef]
91. Zhang, C.; Yan, Q.; Zhang, Y.; Liao, X.; Xu, G.; He, Z. Nondestructive Detection of Fiber Content in Steel Fiber Reinforced Concrete through Percussion Method Coordinated with a Hybrid Deep Learning network. *J. Build. Eng.* **2024**, *86*, 108857. [CrossRef]
92. Kundi, G.M.; Shah, B. IT in Pakistan: Threats & Opportunities for eBusiness. *Electron. J. Inf. Syst. Dev. Ctries.* **2019**, *36*, 1–31.
93. Zhao, J.; Hu, T.; Zheng, R.; Ba, P.; Mei, C.; Zhang, Q. Defect Recognition in Concrete Ultrasonic Detection Based on Wavelet Packet Transform and Stochastic Configuration Networks. *IEEE Access* **2021**, *9*, 9284–9295. [CrossRef]
94. Hu, T.; Zhao, J.; Yan, S.; Zhang, W. Performance Analysis of a Wavelet Packet Transform Applied to Concrete Ultrasonic Detection Signals. *J. Physics* **2021**, *1894*, 012062. [CrossRef]
95. Zeng, Y.; Wang, X.; Xu, M.; Zhong, Y.; Wang, C. Image Denoising for Laser Ultrasonic Inspection of Wire Arc Additive-Manufactured Components with a Rough Surface. *Nondestruct. Test. Eval.* **2023**, *12*, 1407–1433. [CrossRef]
96. Naqiuddin, M.M.; Leong, M.S.; Hee, L.M.; Azrieasrie, M.A.M. Ultrasonic Signal Processing Techniques for Pipeline: A review. *MATEC Web Conf.* **2019**, *255*, 06006. [CrossRef]
97. Arbaoui, A.; Ouahabi, A.; Jacques, S.; Hamiane, M. Concrete Cracks Detection and Monitoring Using Deep Learning-Based Multiresolution Analysis. *Electronics* **2021**, *10*, 1772. [CrossRef]
98. Pawar, P.; Buktar, R. Detection and Classification of Defects in Ultrasonic Testing Using Deep Learning. In *Proceedings of the 2nd International Conference on Recent Trends in Machine Learning, IoT, Smart Cities and Applications: ICMISC 2021*; Springer: Singapore, 2022; pp. 1–15.
99. Sayyar-Roudsari, S.; Shalbaftabar, A.; Damirchilo, F.; Taslimian, R.; Abu-Lebdeh, T.; Hamoush, S.; Yi, S. Defect Classification of Reinforced Concrete Structures with Nondestructive Tests Using Statistical and Machine Learning Methods. *Am. J. Eng. Appl. Sci.* **2024**, *17*, 102–115. [CrossRef]
100. Wu, Y.; Zhang, J.; Gao, C.; Xu, J. Internal Defect Detection Quantification and Three-Dimensional Localization Based on Impact Echo and Classification Learning Model. *Measurement* **2023**, *218*, 113153. [CrossRef]

101. Wang, L.; Yi, S.; Yu, Y.; Gao, C.; Samali, B. Automated Ultrasonic-Based Diagnosis of Concrete Compressive Damage Amidst Temperature Variations Utilizing Deep Learning. *Mech. Syst. Signal Process.* **2024**, *221*, 111719. [CrossRef]
102. Ye, J.; Ito, S.; Toyama, N. Computerized Ultrasonic Imaging Inspection: From Shallow to Deep Learning. *Sensors* **2018**, *18*, 3820. [CrossRef]
103. Khandakar, A.; Chowdhury, M.E.H.; Reaz, M.B.I.; Ali, S.H.M.; Kiranyaz, S.; Rahman, T.; Chowdhury, M.H.; Ayari, M.A.; Alfkey, R.; Bakar, A.A.A.; et al. A Novel Machine Learning Approach for severity Classification of Diabetic Foot Complications Using Thermogram Images. *Sensors* **2022**, *22*, 4249. [CrossRef]
104. Trella, A.L.; Zhang, K.W.; Nahum-Shani, I.; Shetty, V.; Doshi-Velez, F.; Murphy, S.A. Designing Reinforcement Learning Algorithms for Digital Interventions: Pre-Implementation Guidelines. *Algorithms* **2022**, *15*, 255. [CrossRef] [PubMed]
105. Sathiparan, N.; Jeyananthan, P. Predicting Compressive Strength of Cement-Stabilized Earth Blocks Using Machine Learning Models Incorporating Cement Content, Ultrasonic Pulse Velocity, and Electrical Resistivity. *Nondestruct. Test. Eval.* **2024**, *39*, 1045–1069. [CrossRef]
106. Burrascano, P.; Di Schino, A.; Versaci, M. Efficient Estimation of Synthetic Indicators for the Assessment of Nonlinear Systems Quality. *Appl. Sci.* **2024**, *14*, 9259. [CrossRef]
107. Burrascano, P.; Ciuffetti, M. Early Detection of Defects through the Identification of Distortion Characteristics in Ultrasonic Responses. *Mathematics* **2021**, *9*, 850. [CrossRef]
108. Mattsson, P.; Wigren, T. Convergence Analysis for Recursive Hammerstein Identification. *Automatica* **2021**, *71*, 179–186. [CrossRef]
109. Xu, M.; Chen, G.; Tian, Y.T. Identifying Chaotic Systems Using Wiener and Hammerstein Cascade models. *Math Ematical Comput. Model.* **2001**, *33*, 483–493. [CrossRef]
110. Ölmez, M.; Güzeliş, C. Exploiting Chaos in Learning System Identification for Nonlinear State Space Models. *Neural Process. Lett.* **2015**, *41*, 29–41. [CrossRef]
111. Jibril, M.M.; Zayyan, M.A.; Malami, S.I.; Usman, A.G.; Salami, B.A.; Rotimi, A.; Abba, S.I. Implementation of Nonlinear Computing Models and Classical Regression for Predicting Compressive Strength of High-Performance Concrete. *Appl. Eng. Sci.* **2023**, *15*, 100133. [CrossRef]
112. Fang, Q.; Xiong, G.; Zhou, M.; Tamir, T.S.; Yan, C.B.; Wu, H.; Shen, Z.; Wang, F. Process Monitoring, Diagnosis and Control of Additive Manufacturing. *IEEE Trans. Autom. Sci. Eng.* **2022**, *21*, 1041–1067. [CrossRef]
113. Adamu, M.; Haruna, S.I.; Malami, S.I.; Ibrahim, M.N.; Abba, S.I.; Ibrahim, Y.E. Prediction of Compressive Strength of Concrete Incorporated with Jujube Seed as Partial Replacement of Coarse Aggregate: A Feasibility of Hammerstein–Wiener Model versus Support Vector Machine. *Model. Earth Syst. Environ.* **2022**, *8*, 3435–3445. [CrossRef]
114. Adamu, M.; Çolak, A.; Umar, I.; Ibrahim, Y.; Hamza, M. An Intelligent Approach for Predicting Mechanical Properties of High-Volume Fly Ash (HVFA) Concrete. *Civ. Eng. J.* **2023**, *9*, 12–26. [CrossRef]
115. Lin, W.; Jiang, C.; Qian, J. The Identification of Hammerstein Model Based on PSO with Fuzzy Adaptive Inertia Weight. *J. Syst. Sci. Inf.* **2005**, *3*, 32–41.